Efflux-linked Accelerated Evolution of Antibiotic Resistance at a Population Edge

Souvik Bhattacharyya[1*], Madhumita Bhattacharyya[2], Dylan M. Pfannenstiel[1], Anjan K. Nandi[3], YuneSahng Hwang[1], Khang Ho[1] and Rasika M. Harshey[1*]

Affiliations:

[1] Department of Molecular Biosciences and LaMontagne Center for Infectious Diseases, University of Texas at Austin; Austin, TX 78712

[2] Technical University of Munich, Augsburg, Germany

[3] Department of Physical Sciences, Indian Institute of Science Education & Research, Kolkata, India

*Correspondence to either author: souvikut@utexas.edu; rasika@austin.utexas.edu

SUMMARY

Efflux is a common mechanism of resistance to antibiotics. We show that efflux itself promotes accumulation of antibiotic-resistance mutations (ARM). This phenomenon was initially discovered in a bacterial swarm where the linked phenotypes of high efflux and high mutation frequencies spatially segregated to the swarm edge, driven there by motility. We uncovered and validated a global regulatory network that connects high efflux to downregulation of specific DNA repair pathways even in non-swarming states. The efflux-DNA repair link was corroborated in a clinical 'resistome' database: genomes with mutations that increase efflux exhibit a significant increase in ARMs. Accordingly, efflux inhibitors decreased evolvability to antibiotic resistance. Swarms also revealed how bacterial populations serve as reservoir of ARMs even in absence of antibiotic selection pressure. High efflux at the edge births mutants that, despite compromised fitness, survive there because of reduced competition. This finding is relevant to biofilms where efflux activity is high.

KEYWORDS

Antibiotic Resistance, Efflux, DNA repair, *E. coli*, Swarming, Mutation, Evolution, EPI, Necrosignal

INTRODUCTION

Antibiotic resistance is a global health concern and is being labeled a ‘silent pandemic’(Mahoney et al., 2021; Mendelson et al., 2022). Genetic antibiotic resistance can evolve by natural selection when bacteria are exposed to antibiotics (Shallcross et al., 2017; Traxler and Kolter, 2015). This

35 exposure not only allows positive selection of pre-existing mutations but can also activate efflux
36 pumps (Du Toit, 2017). These pumps are diverse, numerous, and critical for several bacterial
37 physiologies including expulsion of intracellular antibiotics (Nishino et al., 2009). When
38 challenged with antibiotic stress, bacteria activate efflux pathways almost ubiquitously (Webber
39 and Piddock, 2003). ARMs (antibiotic-resistance mutations) that increase the efflux of antibiotics
40 are widely described in clinical isolates (Nikaido and Pages, 2012). We report the existence of a
41 genetic network that connects elevated efflux activity to the downregulation of DNA repair. This
42 finding has clinical implications since antibiotic selection pressure in treatment regimens would
43 induce efflux and consequently promote ARMs. Our analysis of a resistome database curated for
44 ARMs in both clinical and non-clinical isolates showed a positive correlation between ARMs that
45 increase efflux and total ARMs in the genome.

46 ARMs are vulnerable to loss in the absence of antibiotic selection pressure because the
47 mutants invariably experience a reduction in fitness. This is because of the essentiality of the
48 cellular targets of antibiotics - transcription, translation, or cell wall biogenesis – processes most
49 often modified by the genetic resistance mechanisms (Kohanski et al., 2010). When competing
50 with susceptible individuals in an antibiotic-free environment, mutations that confer resistance but
51 alter cellular physiology are disadvantageous (Andersson and Levin, 1999; Bottger et al., 2005;
52 Melnyk et al., 2015). This has been demonstrated to be especially true when the density of
53 population (and hence competition) is high (Hibbing et al., 2010; Otto and Whitlock, 1997). And
54 yet, they are seen to persist in dense populations such as biofilms (Steenackers et al., 2016). We
55 report the discovery of a special ecology at the edge of a dense population where ARMs survive.
56 Cells exhibiting high efflux and high mutation frequencies segregate to the edge, where they spawn
57 such mutants.

58 Our model dense population is the *E. coli* swarm, where the bacteria move collectively
59 over a semi-solid surface, powered by flagella (Harshey, 2003; Partridge and Harshey, 2013b).
60 Cells in a swarm grow and divide as they colonize ever-increasing swaths of territory; these cells
61 are physiologically distinct from their planktonic counterparts. Unlike dense biofilms, in which
62 bacteria have reduced metabolism and slow growth (Flemming et al., 2016; Hoiby et al., 2010),
63 swarms are metabolically highly active (Kearns, 2010; Partridge and Harshey, 2013a). An
64 unexpected property of bacterial swarms is their tolerance to a broad class of antibiotics, which
65 dissipates when the bacteria are removed from the swarm and dispersed in liquid (Butler et al.,
66 2010; Kim et al., 2003; Lai et al., 2009). 'Tolerance' and 'persistence' are adaptive physiological
67 mechanisms in bacteria that temporarily either turn down growth or turn up multidrug efflux
68 pumps (Brauner et al., 2016). Swarms exhibit elevated efflux and ROS catabolism and decreased
69 membrane permeability even in the absence of antibiotic exposure, suggesting perhaps an
70 anticipatory program to survive an encounter with antibiotics. ROS stress is known to be generated
71 by high cell densities (Chang et al., 2002; Dukan and Nystrom, 1998) and by increased energy
72 utilization expected during efflux (Anes et al., 2015; Fang, 2011; Imlay, 2013). When confronted
73 with antibiotics, swarms further elevate both efflux and ROS catabolism. One of the proximate
74 causes of this elevation is release of a 'necrosignal' from antibiotic-induced death of a sub-
75 population. The antibiotic tolerance-enhancing factor was identified as being a part of an efflux
76 pump itself: AcrA, a periplasmic component of the AcrAB-TolC RND efflux pump, is released
77 from dead cells and signals live cells by interacting with TolC in the outer membrane to enhance
78 drug efflux as well as to induce expression of many other efflux pumps (Bhattacharyya et al.,
79 2020). We have called this phenomenon 'necrosignaling' and have demonstrated its existence in

80 other Gram-negative as well as Gram-positive bacteria (Bhattacharyya et al., 2020). High efflux
81 in swarms has parallels with ARMs that increase efflux in clinical settings.

82 We report here the convergence of several phenomena that create a high-evolvability niche
83 at the advancing edge of an *E. coli* swarm. Cells at the edge are engaged in high efflux, likely for
84 bringing in hard-to-get iron on a surface terrain. High efflux generates ROS stress, which may play
85 a role in activating a regulatory pathway that connects efflux to downregulation of specific DNA
86 repair genes, producing a mutator phenotype. Motility plays another important role in assisting
87 this phenotype to 'surf' to the edge of the swarm where chances of fixation of unfit mutations are
88 expected to be high due to reduced competition. Edge cells incur more cell death as well, releasing
89 the necrosignal AcrA, which stimulates efflux further. We show that the mutator phenotype can
90 be suppressed by inhibitors that target both AcrA and the efflux pump.

91

92 **RESULTS AND DISCUSSION**

93 **Swarms Downregulate DNA Repair and Show High Evolvability to Antibiotic Resistance**

94 Compared to planktonic populations, *E. coli* swarms intrinsically upregulate efflux and ROS
95 catabolism pathways (Bhattacharyya et al., 2020). A study showing a correlation between
96 increased efflux pump activity and downregulation of the DNA repair gene *mutS* in planktonic
97 cells of *E. coli* (El Meouche and Dunlop, 2018), led us at first to re-examine our *E. coli* RNA seq
98 data from swarms, which showed a 3-6 fold downregulation of eight DNA repair genes – *dinB*,
99 *holA*, *lexA*, *mug*, *mutM*, *mutS*, *recC*, and *ung* (Figure 1A inset and Figure S1A). These genes are
100 broadly involved in mismatch and nucleotide-excision repair, predicting a mutator phenotype. This
101 was tested by examining for the presence of mutants resistant to the antibiotic Kanamycin (Kan^R)

102 in the swarm, using a modification of the border-crossing assay originally designed to demonstrate
103 antibiotic tolerance in swarms (Butler et al., 2010). *E. coli* can swarm collectively on the surface
104 of media solidified with ~0.5% agar (videos S1, S2), but will swim as individuals within softer
105 agar (0.3%) (Partridge and Harshey, 2013a). Swimming bacteria are effectively in a planktonic
106 state, so we will henceforth use S and P symbols to denote swarm and planktonic states. In the
107 assay, a 2-chamber Petri dish filled with swarm media contains antibiotic in only one chamber;
108 bacteria that begin swarming in the no-antibiotic chamber and arrive at the separating border, will
109 attempt to cross over and colonize the antibiotic chamber. To detect individual bacteria harboring
110 Kan^R mutations that arose within the swarm, we modified this assay to contain swim media with
111 Kan in the right chamber (Figure 1B schematic; S to P setup). A control set-up for observing such
112 mutants arising in the P population had swim media in both chambers (P to P setup).

113 Kan^R mutants were recovered in both P-P and S-P set-ups (Figure 1C-D). The distinct
114 points along the border from where the Kan^R swim 'flares' emerge report on the physical location
115 of the original mutant in the S or P population, which then colonizes the area on the right. Kan^R
116 mutants were recovered at a higher frequency per plate in S-to-P compared to P-to-P setups (Figure
117 1C-D and Figure S1B). A total of 32 Kan^R mutants were collected, 25 that arose from S-P setup,
118 and 7 from the P-P setup. To determine the mutation frequency (MF) accurately, we measured
119 resistance to the antibiotics Rifampicin (Rif) and Kan (Fowler et al., 1994; Kapoor et al., 2019;
120 Miller et al., 1977) in both populations. Compared to P cells, S cells of *E. coli* exhibited a ~5-fold
121 higher MF (Figure 1E). To test if this was a general feature of S cells, MFs were also calculated
122 for S cells of *Bacillus subtilis* (Figure 1F) and *Pseudomonas aeruginosa* (Figure S1C), which
123 showed ~8- and ~7-fold MF increases, respectively, compared to their P counterparts.

124 Differences in the intensity and size of the flares that emerged in the *E. coli* set up in Figure
125 1C, could be indicative of differences in the proficiency of growth and/or motility of the mutants.
126 We therefore examined these parameters closely in all 32 mutants, as well as identified the
127 mutations by whole-genome sequencing. Mutants derived from P cells (P1-7) were uniformly poor
128 in motility (M) (Figure 1G), whereas those from S cells varied in this property, some moving even
129 better than wild type (WT) (S1-25) (Figure 1G and Figure S1D). P-derived mutants were also
130 uniformly poor in growth (G) (group 4 in Figure 1G and Figure S1E), whereas S-derived mutants
131 clustered into four distinct groups, some growing as well as WT (groups 1-4 in Figure 1G and
132 Figure S1E). DNA sequencing revealed an enrichment of mutations in three genes – *fusA, cydA,*
133 *dgcJ* - across the mutant set (Figure 1H). *fusA* encodes elongation factor G (EF-G), which is a
134 known source of Kan^R mutants (Voorhees and Ramakrishnan, 2013) as Kan inhibits translation by
135 binding to the A site in the 30S ribosomal subunit, blocking EF-G catalyzed translocation. *cydA*
136 encodes subunit I of cytochrome bd-I terminal oxidase. Kan^R mutations previously isolated in *cydA*
137 (Hol et al., 2016) resulted in decreased PMF and were inferred to have decreased Kan uptake
138 (Becker and Cooper, 2013). The third gene *dgcJ* is a putative cyclic di-GMP synthase and has no
139 reported connection to Kan^R, but is expected to increase motility (Jenal et al., 2017; Pesavento et
140 al., 2008). To test if these mutations directly conferred the Kan^R phenotype, wild-type copies of
141 all three genes were overexpressed in four representative isolates, yielding the following results.
142 Overexpression of *fusA* caused Kan^R to diminish only in strains with *fusA* mutations (Figure 1I,
143 S1&S2 set; Figure S1F), while *cydA* overexpression reduced Kan^R only in strains with *cydA*
144 mutations (Figure 1I, S6&S9 set; Figure S1F). Overexpression of *dgcJ* did not abrogate the Kan^R
145 phenotype in strains with *dgcJ* mutations (Figure 1I, S6&S9 set), but greatly reduced swimming
146 motility of all strains tested, including that of WT (Figure 1J, swim; Figure S1G), consistent with

147 the known role of c-di-GMP (the enzymatic output of DgcJ) in inhibiting motility. In summary,
148 these experiments confirm that mutations in *fusA* and *cydA* confer Kan^R, whereas DgcJ may have
149 a specific role in swarming motility as indicated by the abundance of *dgcJ* mutants in isolates only
150 from the S samples.

151 The relationship of *cydA*, *fusA* and *dgcJ* mutations in promoting Kan^R and motility is
152 sketched Figure 1K, based on literature reports. Mapping the mutations associated with the three
153 genes onto the known or predicted structures of these three proteins showed that for EF-G, most
154 mutations mapped to residues known to affect the translocation of the ribosome (Zhou et al., 2014),
155 but the two that map to domain I and II of EF-G, respectively (Connell et al., 2007), have no known
156 connection with translocation (R146 and T393) (Figure 1L). For CydA, the two mutants isolated
157 were at positions not previously associated with Kan^R (Allison et al., 2011) (Figure 1M). For DgcJ,
158 four were in the predicted enzyme active site (Hengge, 2009), while one mapped to the predicted
159 periplasmic sensory domain (Figure 1N).

160 In summary, the results in this section show that *E. coli* swarms downregulate a set of eight
161 specific DNA repair genes and expectedly, show higher MFs. This observation is not unique to *E.*
162 *coli* swarms, as high MFs are also observed in *B. subtilis* and *P. aeruginosa* swarms. A large
163 majority of Kan^R mutants recovered from edge of *E. coli* swarms are accompanied by mutations
164 that improve their motility in the swarm.

165

166 **Downregulation of Mismatch and Base Excision Repair Pathways Contributes to the Higher**
167 **MFs of Swarm Cells**

168 A detailed analysis of all the mutations recovered in the genomes of the 32 mutants (Figure 1G)
169 revealed that of 501 total mutations identified, A→G and T→C changes were each ~5% lower in
170 S compared to P isolates, whereas T→G and C→T changes were each ~2-3% higher in S (Figure
171 2A and Figure S2A). Overall, transition mutations decreased by ~11% and transversions increased
172 by ~8% in S isolates (Figure 2B, whole genome). Considering only the mutations in genes
173 conferring Kan^R – *fusA* and *cydA* – transitions decreased ~ 21% and transversions increased ~6%
174 in S compared to P cells (Figure 2B, Kan^R). Two other types of mutations isolated across the
175 genome were indels. Of these, insertions ranging from 4 -11 bp were found in *dgcJ* whereas
176 deletions from 6-9 bp were found in *cydA*. We found no bias in the distribution of mutations in
177 coding or non-coding regions (Figure 2B and Figure S2B).

178 To test which repair pathway might be responsible for the mutations recovered in S cells,
179 these cells were exposed to mutagenic agents handled by the various pathways (Figure 2C).
180 Acidified nitrite, a stressor for base excision, nucleotide excision, and mismatch repair pathways
181 (Davies et al., 2011; Kurthkoti et al., 2008), significantly reduced the growth of S cells (Figure
182 2D-E). On the other hand, S cells survived better under the stress of hydrogen peroxide, an ROS
183 agent affecting multiple DNA repair pathways (Figure 2D-E), consistent with the elevated
184 expression in S cells of genes involved in scavenging ROS (Bhattacharyya et al., 2020). Bleomycin
185 and UV light exerted significant but similar growth reduction in both P and S cells (Figure 2D-E)
186 suggesting that DNA break repair pathways are not likely to be altered in S cells. We infer from
187 these results that the downregulation of mismatch repair (MMR) and base excision repair (BER)
188 pathways are likely contributing to the higher MF of S cells.

189 To further identify the specific pathways whose malfunction may have produced these
190 mutations, we focused on the eight DNA repair genes (Friedberg, 2006; Rosenberg et al., 2012)

191 downregulated in S cells (see Figure 1A), and overexpressed them using clones selected from the
192 *E. coli* ASKA ORF-eome. Only clones of *mutS*, *mutM*, and *ung* significantly reduced MFs, which
193 were now comparable to the MF of P cells (Figure 1E and 2F); MutS is an MMR protein, MutM
194 is a formamidopyrimidine-DNA glycosylase and Ung is an uracil-DNA glycosylase. The latter
195 two are involved in BER pathways (Figure 2C).

196 To identify the source of the damage contributing to the high MF of S cells, we monitored
197 intracellular nitrite and peroxide levels using commercial kits. Levels of nitrite were similar
198 between S and P cells, while intracellular peroxide levels were elevated in S cells (Figure 2G).
199 Introduction of clones of known ROS catabolism genes *katE* and *sodB*, lowered the peroxide levels
200 in S cells (Figure 2G). These results imply that despite the increase in expression of ROS
201 catabolism genes observed in S cells (Bhattacharyya et al., 2020), these cells still experience ROS
202 stress.

203 In summary, three lines of evidence – the nature of mutations recovered in S cells, the
204 susceptibility of S cells to mutagens handled by MMR and BER pathways, and the elevated cellular
205 peroxide levels in these cells, suggests that the high MF of S cells likely arises from both high
206 cellular redox stress and decreased expression of the MMR and BER genes *mutS*, *mutM* and *ung*,
207 which are known to handle DNA damage by ROS.

208

209 **A Global Regulatory Connection Between Efflux and DNA Repair**

210 Efflux pump expression is tightly regulated by a vast network of regulators (Sun et al., 2014). To
211 determine if efflux and DNA repair networks (Milanowska et al., 2011) were genetically
212 connected, we took the bottoms-up approach summarized in Figure 3A. The regulatory

213 connections between genes (nodes) in these two sets of pathways were interrogated by performing
214 a nodal analysis of the three genes uncovered in this study - *ung*, *mutS*, and *mutM* - taken from the
215 *E. coli* MG1655 curated genetic network Ecocyc (Keseler et al., 2011). We searched for regulatory
216 paths connecting these three peripheral nodes to the efflux pump gene network, validating them
217 by correlation of expression of gene-pairs using data from COLOMBOS [normalized *E. coli* gene
218 expression data derived from 4000 experimental sets; (Moretto et al., 2016)]; we used our RNA
219 seq data (Bhattacharyya et al., 2020) as an additional guide (Figure 3B-C and Figure S3A). From
220 all the genes participating in these regulatory paths (Figure 3D top), only those gene pairs showing
221 significant correlation coefficients from this analysis were considered (Figure 3C top), and are
222 highlighted in Figure 3D (bottom) (see Figure S3B for paths that failed validation). The analysis
223 revealed that downregulation of *mutS* and *ung* was controlled by *rpoS* via *sdsR* and *cpxR* nodes
224 respectively, while downregulation of *mutM* was controlled by *crp* via *rpoH*. Therefore, *rpoS* and
225 *crp* were the major nodes seen to connect efflux and DNA repair. RpoS is an alternative sigma
226 factor, which controls the expression of hundreds of genes that protect the cell from stress and help
227 survive nutrient deprivation (Landini et al., 2014), while CRP is a global transcription regulator of
228 many genes mostly involved in energy metabolism (Grainger et al., 2005). We note that our
229 analysis used datasets from thousands of experimental conditions not specific to *E. coli* swarms,
230 so the identified links are evolutionarily wired and the consequences of their perturbation should
231 be relevant in most niches these bacteria occupy.

232 What upstream signal might be relayed via the *rpoS* and *crp* nodes? High efflux pump
233 activity is associated with various stress responses (Rosner and Martin, 2013). Efflux consumes
234 an enormous amount of energy [ATP, PMF or Na+/H+ antiport systems drive various pumps (Du
235 et al., 2018)] (Fang, 2011; Imlay, 2013). Like efflux, flagella biosynthesis and rotation during

236 swarming also consume both PMF and ATP (Chevance and Hughes, 2008; Gabel and Berg, 2003).
237 A high metabolic rate would be required to sustain a high PMF, which in turn would lead to high
238 intracellular ROS. This was already inferred from gene expression data (Bhattacharyya et al.,
239 2020), and demonstrated experimentally as well (Figure 2G). ROS are also produced by high cell
240 densities (Chang et al., 2002; Dukan and Nystrom, 1998). Could the two global regulators RpoS
241 and Crp identified in our analysis likely respond to ROS stress? This hypothesis was tested by
242 measuring the effect on MF of deleting some of the regulators identified in the nodal analysis (*rpoS*
243 and *crp* themselves were not deleted to avoid pleotropic effects (Ishihama et al., 2016)). Deletion
244 of the major efflux regulators *marA* and *evgA* (Du et al., 2018) reduced MF, while their
245 overexpression increased it (Figure 3E). A double deletion of *marA* and *evgA* decreased MF of S
246 cells almost to the level of P cells (Figure 3E). The MarA regulon increases the expression of many
247 efflux genes including *acrA*, *acrB*, and *tolC*. Similarly, EvgA controls the expression of efflux
248 genes *acrD* and *mdtEF* (Du et al., 2018). To test whether the effect of these regulators on MF are
249 pleiotropic or whether they occur via the genes they are known to regulate, we overexpressed *marA*
250 in an Δ*acrB* strain, and *evgA* in an Δ*acrD* strain; in neither case did MF increase, showing that
251 MarA and EvgA effects are routed through their specific genetic circuits. We conclude from both
252 the nodal analysis and the experimental data presented, that the increased activity of efflux pumps
253 itself downregulates specific DNA repair genes.

254 In summary, the experiments in this section show that the global regulators RpoS and Crp
255 link specific DNA repair genes to efflux pump regulators. The results imply that these genetic
256 links have been integrated into a network through evolutionary forces that increase mutagenesis
257 and hence evolvability when bacteria experience high efflux-related ROS stress – an evolutionary
258 model similar to other widely reported modes of stress-induced mutagenesis (Fitzgerald et al.,

259 2017; MacLean et al., 2013; Ram and Hadany, 2014). Given that high efflux is a temporary state
260 operative only during swarming, we suggest that the ultimate cause (Laland et al., 2011; Mayr,
261 1961), i.e. long-term or evolutionary importance of this reversible state is acquisition of genetic
262 resistance.

263

264 **The Efflux-DNA Repair Network is Clinically Relevant to the Rise in Antibiotic Resistance**

265 We have shown thus far that high-efflux leads to a mutator phenotype, which in turn creates genetic
266 resistance to antibiotics or ARMs. Do these findings have any clinical significance? Mutations that
267 increase efflux are known to provide resistance to antibiotics (Li et al., 2015). However, the MF
268 data for clinical isolates are scarce. Based on the findings in Figure 3, we can expect to find a
269 linkage between mutations that increase efflux and accumulation of ARMs in genomes of bacteria.
270 To examine this, we used the Comprehensive Antibiotic Resistance Database (CARD) (Alcock et
271 al., 2020), which catalogues ARMs for bacteria from both clinical and non-clinical sources. We
272 analyzed only the resistome of *E. coli* (Figure 4A, Figure S4A-B). The data showed that the
273 occurrence of efflux ARMs per genome follows a distribution pattern that is completely different
274 from that of non-efflux ARMs. The fraction of genomes with efflux ARMs peaked at 17 mutations
275 per genome and showed a gradual decrease up to 42 mutations per genome, but the fraction with
276 non-efflux ARMs peaked at 1 mutation and started a steep decline at 4 mutations per genome
277 (Figure 4B). More importantly, a strong positive correlation was found between efflux ARMs vs
278 total ARMs in a genome (Figure 4C), supporting our hypothesis that efflux-promoting mutations
279 tend to lead to more ARMs. Similar calculations with other categories of mutations did not show
280 this association (Figure 4D-F, Figure S4C-E). A Spearman correlation matrix among these
281 categories shows efflux and total mutations to be the only significantly correlated categories

282 (Figure 4G, Figure S4F). These data suggest that, like in case of S cells, high efflux increases the
283 rate of evolution of ARMs even in clinical settings, and consequently multidrug resistance.

284

285 **The Mutator Phenotype of Swarms Can be Inhibited by Efflux Pump Inhibitors**

286 The high efflux of swarm cells is further stimulated by the necrosignal AcrA, released upon death
287 of a subpopulation (Bhattacharyya et al., 2020). It follows that AcrA addition should increase MF.
288 We therefore incubated both P and S cells with purified AcrA and observed a significant increase
289 of MF in S cells, but only a modest increase in P cells (Figure 5A). Conversely, inhibiting AcrA,
290 which is an essential periplasmic component of the AcrA-TolC RND efflux pump, should not only
291 reduce antibiotic outflow, but should also suppress the mutator phenotype. Using as a guide a
292 recent study which identified several small molecules that target AcrA (Abdali et al., 2017), we
293 selected three compounds – Novobiocin (Nov), Clorobiocin (Clo), and NSC60339 (Figure 5B-C)
294 to study their effect on MF. Nov and Clo are both aminocoumarins that also target DNA gyrase
295 activity (Gross et al., 2003) To circumvent this effect, we overproduced in the cells a *gyrB* mutant
296 (R136L) conferring resistance to both Nov and Clo (Gross et al., 2003) (Figure S5A-C). We then
297 treated both WT and Δ*acrA* S cells expressing $gyrB^{R136L}$ with all three inhibitors in the presence
298 or absence of externally added AcrA. Inhibition of AcrA was observed to decrease MF for all three
299 compounds tested (Figure 5D-E). The increase of MF seen in WT S cells (i.e. without the *gyrB*
300 allele) treated with Nov and Clo alone (Figure 5D, WT columns) is consistent with the idea that
301 antibiotics increase DNA damage from redox stress (Dwyer et al., 2014) (Imlay, 2013). In contrast
302 to Nov and Clo, the compound NSC60339 that solely targets AcrA to inhibit both efflux and
303 necrosignaling, decreased MF even in WT. Among the three compounds tested, NSC60339

304 showed the best activity in decreasing both efflux- and necrosignal-mediated MF in all strain
305 backgrounds (Figure 5D, NSC).

306 In summary, we have shown that drugs targeting both efflux and AcrA reduced the MF of
307 swarms, opening up new possibilities for interfering with evolvability to drug resistance in clinical
308 settings. We note that a wide variety of bacteria, both Gram positive and Gram negative, show
309 necrosignaling (Bhattacharyya et al., 2020). In the case of *E. coli*, the necrosignal AcrA happens
310 to be a component of the efflux pump, making these inhibitors doubly effective. The nature of
311 other necrosignals remains to be investigated.

312

313 **A Role for Efflux in Iron Acquisition: Spatial Heterogeneity in Efflux, Redox, and Cell Death**

314 Why do swarms intrinsically exhibit high efflux? Two lines of thought led us to examine whether
315 the primary role of efflux is in obtaining iron from the environment. A variety of studies, including
316 the finding that iron acquisition systems are upregulated, have shown that the bacteria are iron-
317 starved on the surface (Inoue et al., 2007; Lin et al., 2016; McCarter and Silverman, 1989;
318 Partridge and Harshey, 2013a; Wang et al., 2004). Iron-scavenging systems encode high-affinity
319 iron-binding siderophores, which are secreted into the extracellular matrix to bring iron back in
320 (Kramer et al., 2020; Wilson et al., 2016). Efflux pumps are crucial for siderophore secretion
321 (Bleuel et al., 2005; Henderson et al., 2021). If the high efflux activity of swarmers is being
322 employed to obtain iron as the swarm advances into new territory, center and edge zones of a
323 swarm should differ in their amount of siderophores and free iron. Classical staining methods
324 (Schwyn and Neilands, 1987) to monitor siderophores could not be directly used on the swarm
325 plate. We therefore lifted cells from different zones on swarm plates (Figure 6A), to measure

326 siderophores (Schwyn and Neilands, 1987) and iron (Oviedo et al., 2003). The data are plotted as
327 a circular bubble plot to capture the radially symmetric nature of the *E. coli* swarm (Figure 6B-C).
328 Siderophore levels were high at the edge and low at the center, while free iron showed a reverse
329 trend.

330 If cells at the advancing edge are engaged in efflux for iron acquisition, would the edge
331 cells experience higher ROS levels and perhaps also cell death as a consequence? Initially, ROS
332 levels were measured in the entire swarm using the redox-sensitive biosensor roGFP, which
333 increases its fluorescence upon oxidation of specific cysteines by ROS moieties inside the cell
334 (Morgan et al., 2011; van der Heijden et al., 2016). S cells were observed to have ~ 6-fold increase
335 in fluorescence intensity compared to P cells (Figure 6D, Figure S6A). The fluorescent signal
336 binned into two distinct sets (Figure 6E) and was noisier (Figure S6B) than that in P cells. The
337 frequency distribution of S cell fluorescence is shown in Figure 6E (graph). We then isolated and
338 measured roGFP intensity of cells separately from the center and edge of the swarm (Figure 6F-
339 G, Figure S6C-E). The center cells showed a single prominent peak of fluorescence indicating a
340 homogeneous population with respect to ROS levels (Figure 6F graph). Edge cells on the other
341 hand were more heterogeneous and displayed two peaks (Figure 6G graph). In addition, edge cells
342 had ~5-fold more mean fluorescence compared to the center cells (Figure S6F).

343 To test whether the redox heterogeneity is a direct result of efflux activity, roGFP
344 containing S cells were stained with Nile red, which is an indicator dye for efflux (Bohnert et al.,
345 2010) - more Nile red accumulation indicating lower efflux. An anticorrelation between roGFP
346 and Nile red signals was observed (Figure 6H-J, middle and right, and Figure S6G), which
347 followed an exponential decay (Figure 6K). Consistent with the bimodal distribution of ROS
348 profiles, S cells also exhibited a bi-modal distribution in efflux, which indicated the presence of

349 two different efflux cell-types (Figure 5I). A Nile red efflux assay confirmed that edge cells have
350 ~40% higher efflux activity than center cells (Figure S6H). To evaluate whether cellular energetics
351 and respiration are responsible for efflux-driven ROS stress, the redox dye 5-cyano-2,3-ditolyl
352 tetrazolium chloride (CTC) (Rodriguez et al., 1992) was used to stain the roGFP cells. Presence
353 of CTC-formazan is a direct indicator of electron transport chain activity. There was a significant
354 positive correlation between CTC and ROS signals (Figure 6K-M and Figure S6G). Again, the
355 CTC signal revealed two intensity peaks (Figure 6L).

356 To test the deduction that high ROS causes more death, we treated S cells with a live-dead
357 stain and indeed observed ~4-6-fold higher death within swarms compared to P populations
358 (Figure 6N; Figure S6A). Edge cells specifically had ~3-fold higher death compared to center
359 (Figure 6O).

360 In summary, high efflux activity at the edge is likely employed for mitigating iron
361 starvation experienced during surface growth, providing an explanation for why S cells engage in
362 more efflux than P cells. In addition to the genetic association between high efflux and an increase
363 in MF, ROS production from efflux itself leads to cellular damage. The data demonstrate that
364 swarm edge and center cells are phenotypically distinct and spatially segregated with respect to
365 efflux and death, with edge cells conducting more efflux and undergoing more death. Cell death
366 is expected to release the necrosignal AcrA, which would further stimulate efflux, and therefore
367 MF (Figure 5A). A high-efflux physiology at the edge would be an added bonus while swarming
368 in relevant habitats where the advancing edge would be expected to be at the forefront of an
369 encounter with antibiotic-producing microbes.

370

371 **Phenotype Surfing: an Evolutionary Mechanism for Breeding Mutants that Survive in the**
372 **Absence of Selection**

373 Thus far, we have seen a striking segregation of various linked phenotypes – increased efflux, high
374 ROS stress, and more cell death – at the edge of the swarm. These phenotypes are also directly
375 correlated with high MF and with evolution of antibiotic resistance mutations. Evolution does not
376 favor high MF because of its deleterious effects in general, especially when the population is dense
377 (Krasovec et al., 2014; Krasovec et al., 2017; Lynch et al., 2016; Sprouffske et al., 2018); in fact,
378 increasing the density of planktonic cultures actually decreases MF (Krasovec et al., 2014).
379 Compensatory mutations that rescue the reduced fitness of such mutants can arise (Bjorkman et
380 al., 2000), but could take a few tens of generations to appear (Sousa et al., 2012), greatly increasing
381 the chances of elimination of the original resistance mutation from the population (Melnyk et al.,
382 2015). So how does the swarm support high MF?

383 To address this enigma, we first measured the rate of evolution in swarms by applying the
384 concept of 'evolvability' E (Pigliucci, 2008), which is the ability of a biological system to produce
385 phenotypic variation that is both heritable and adaptive (Payne and Wagner, 2019). We defined E
386 as a product of mutation frequency (MF) and total size of the population (N). Since N is dependent
387 on the growth rate G of a population, we measured G for both S and P cells (Figure S7A). A 3D
388 plot of these values showed that S cells have an unexpectedly better E than P cells, suggesting that
389 S cells are indeed on a different evolutionary trajectory (Figure 7A). Two observations further
390 support this view. First, we found frequent co-occurrence of two Kan^R-conferring mutations in S
391 isolates (Figure 1H) in the relatively short selection window of our experiments (24-48 h), an event
392 that is highly unlikely in P cells (Elena and Lenski, 2003), where such mutants were indeed not

393 observed. Second, majority of the Kan^R mutants (Figure 1C-D) had a reduced growth rate, hence
394 lowered fitness (Figure 1G).

395 Deleterious or neutral mutations that are normally lost by Darwinian forces, have a higher
396 chance of becoming randomly fixed by genetic drift (Lynch et al., 2016), which is high at the edges
397 of an expanding population (Hallatschek and Nelson, 2008). Indeed, it has been shown that
398 favorable mutations can become fixed at the edge via a genetic drift-based mechanism called 'gene
399 surfing' (Hallatschek and Nelson, 2008). Using similar principles, we propose a 'phenotype
400 surfing' model where the unfavorable phenotype of high MF has an increased chance of survival
401 at the swarm edge. To test this outcome experimentally, we measured the MFs of center and edge
402 cells as before. The data clearly showed that edge cells have ~6-fold higher MF compared to center
403 cells (Figure 7B). In addition, motility within the swarm would affect genetic drift because faster
404 motility would increase the probability of cells reaching the swarm edge (videos S1, S2) where the
405 chances of drift are high (Hallatschek and Nelson, 2008). Indeed, a significantly higher motility
406 was observed in edge cells when compared to center cells (Figure 7C, Figure S7B-G, and 'Aspect
407 Ratio' in Supplementary text; see also video S3). The model is also supported by data in Figure 1,
408 where a majority (~70%) of the Kan^R mutants isolated from the swarm edge had secondary
409 mutations in *dgcJ*, which specifically enhance swarming motility, implicating their improved
410 motility in transporting Kan^R mutations to the front of the expanding swarm. That these mutations
411 occurred within the edge population and were not simply carried there from the center, is attested
412 to by the observation that the mutants were all unique (Figure 1H); had they arisen earlier, one
413 would expect to see many that inherited the exact same Kan^R-related mutation. Another line of
414 support for the model comes from the observed heterogeneity of fitness costs associated with the
415 Kan^R mutations (Figure 1G, S1E, groups 1-4). The data show that mutants with low fitness

survived in the swarm despite its dense nature, and were recovered at edge where a favorable selection condition was present – in this case Kanamycin.

Figure 7D summarizes the 'phenotype surfing' mechanism derived from the findings reported in this and other sections, and explains how an unfavorable phenotype can increase its survival frequency at the edge. The mechanism is supported by data showing that cells in a swarm are spatially segregated with respect to phenotypes such as MF (Figure 7B) and efflux (Figure S6H) and that motility plays a role in delivering these phenotypes to the edge. Spatial segregation of these phenotypes may be beneficial to the entire colony in two ways. First, the effective population size (Husemann et al., 2016) of a swarm harboring individuals with high genetic relatedness is substantially high. This can support high rates of death as many individuals would still survive. Second, in case of sudden extinction events in the environment that could cause population bottlenecks (Libby and Rainey, 2011), at least some of the spatially segregated individuals would have a better chance of survival. Thus, a perfect storm of events accruing at the edge creates an environment that sustains otherwise unfavorable mutations. The edge phenotype may well be applicable to biofilms if the cells here are engaged in high efflux (Alav et al., 2018). *B. subtilis* biofilms have been demonstrated to have a heterogeneity that includes a special edge function (Larkin et al., 2018).

CONCLUSIONS

Bacterial swarms provide an excellent platform for studying both the biology and the physics of collective motion and of co-operative behavior. Moving as a dense pack bestows swarmer (S) cells with many survival advantages, but the one we focus on in this study is their temporary capacity to live through antibiotic concentrations that would be lethal if the same bacteria were growing in

439 a planktonic (P) state. At least two swarm features help account for this capacity in *E. coli*: an
440 altered S cell physiology that enables high drug efflux, and a mechanism to further elevate efflux
441 upon encountering antibiotics by necrosignaling. The present study reveals several unexpected
442 facets of the relationship between efflux and DNA repair, of segregation of motile cells with high
443 efflux to the edge of the swarm likely for iron acquisition, of higher cell death and resultant high
444 mutation frequencies (MF) of edge cells. The advancing edge therefore becomes a microcosm for
445 generation and survival of otherwise unfavorable mutations, a novel evolutionary phenomenon we
446 have called 'phenotype surfing'.

447 We suggest that the initial condition that sets up the special ecology at the swarm edge is
448 highly motile cells in the population that drive swarm expansion. These cells are also highly
449 metabolically active because motility consumes both PMF and ATP, two energy sources that are
450 also required for efflux. The necessity to acquire iron at the advancing edge therefore favors both
451 phenotypes at the edge because siderophores are secreted via efflux; thus, both phenotypes are
452 favored to expand. Upregulation of efflux brings with it a downregulation of MMR and BER
453 pathways via a network of genetic interactions that appear to respond to the expected ROS stress
454 in the phenotypes segregated at the edge. Dysfunction of DNA repair increases MF. In addition,
455 ROS stress brings with it the risk of cellular damage and collateral death, leading to release of the
456 necrosignal that further increases efflux and hence MF. Mutants that would otherwise have been
457 lost in the interior of the swarm, circulate to the edge and survive there due to decreased
458 competition and increased genetic drift. The positioning of the mutants at the edge provides them
459 an opportunity for range expansion when conditions are ripe, and hence high evolvability to ARMs
460 among other selection forces. Thus, phenotype surfing is a surprising mechanism for evolution in
461 motile bacterial populations, which could in principle also work at the edges of biofilms. In

462 addition to this discovery, our study also provides clues for how to interfere with high evolvability
463 to ARMs.

464

465 **ACKNOWLEDGEMENTS**

466 We thank Jeffrey Barrick for critical comments. We also thank Brett Finlay for kindly sending us
467 the roGFP plasmid. This work was supported by Public Health Service Grants GM118085 and
468 AI158295 to R.M.H.

469

470 **AUTHOR CONTRIBUTIONS**

471 Conceptualization, S.B. and R.M.H.; Methodology, S.B., and R.M.H; Software, S.B., M.B.,
472 A.K.N, and D.M.P; Formal Analysis, S.B., M.B., and A.K.N; Investigation, S.B., D.M.P, and
473 Y.H.; Resources, S.B., M.B, K.H, and A.K.N; Writing – Original Draft and Writing –Review &
474 Editing, S.B. and R.M.H.; Visualization, S.B., M.B, and R.M.H., Supervision and Project
475 Administration, S.B. and R.M.H.; Funding Acquisition, R.M.H.

476

477 **DECLARATION OF INTERESTS**

478 The authors declare no competing interests.

479

480 **FIGURE LEGENDS**

481 **Figure 1. Swarms Downregulate DNA Repair and Show High Evolvability to Antibiotic**
482 **Resistance**

483 (A) Log2-fold change (FC) in expression of efflux and DNA-repair genes in *E. coli* swarm cells;
484 E: efflux, D: DNA repair. Inset: DNA-repair genes downregulated more than 1.5 log2-fold.

485 (B) Border-crossing assay schematic. S: swarm, P: swim; Kan = 25u/ml Kanamycin or Kan^{25}.
486 Bacteria are inoculated in the left no-Kan chamber.

487 (C-D) WT *E. coli* inoculated on the left on either swarm (C) or swim (D) media, crossed the border
488 into Kan^{25} swim media. Representative plates show the emergence of Kan-resistant (Kan^{R})
489 swimmers. Color-coded circles mark distinct phenotypes (see H): Lines between circles indicate
490 the lineage of mutants from WT.

(E-F) Mutation frequencies (MF) of S (blue) and P (red) cells of (E) *E. coli* and (F) *B. subtilis*, measured by resistance to Rifampicin (Rif^{50}) and Kan^{50}. Each black circle is an experimental replicate. [**$p < 0.01$, Mann-Whitney test]

(G) Heat map showing the growth G, and motility M, of Kan^R mutants from C-D, compared to WT. S1-25 were derived from C and P1-7 from D. The clusters of isolated mutants are indicated as 1-4 matching mutant color codes from (C-D)).

(H) Summary of mutations from the individual isolates listed in G scaled to the *E. coli* genome in Mb (bottom). Syntenic mutations in the 3 indicated genes were recovered frequently. White and black boxes = inter- or intragenic mutations.

(I-J) Comparison of growth (I) of indicated mutant and WT strains in Kan^{25} media, and motility (J) in swim media. *f, c, g* indicates complementation with plasmids expressing *fusA*, *cydA*, *dgcJ*; Δ, Δ*dgcJ*. [***$p < 0.001$, Wilcoxon rank sum test]

(K) A schematic summarizing possible effects of recovered mutations in *fusA*, *cydA*, *dgcJ*. (1) *cydA* mutations reduce PMF which may decrease Kan uptake. (2) *fusA* mutations reverse the translation inhibition by Kan. *dgcJ* mutations are expected to reduce c-di-GMP and increase motility.

(L-N) Structures of (L) EF-G (*fusA*; magenta) [PDB:4V7D], (M) CydA [PDB:6RKO], and (N) DgcJ [Alphafold]. Red: mutations in active site (residues 423-427); black: mutations in the predicted sensory domain. In each gene, multiple mutations from different S-P isolates map to the same site.

Figure 2. Downregulation of Mismatch and Base Excision Repair Pathways Contributes to the Higher MFs of Swarm Cells

(A) Heatmaps showing percentages of different types of mutations found in P and S mutants. WT nucleotides are on the left column, and rows show mutations in P1-P7 and S1-S25 isolates (Figure 1G). (B) A comparison of the percent changes (Y-axis) in types of mutations in S and P isolates. Transitions (Ts), Transversions (Tv), Insertions (In) and Deletions (Del) are color coded as indicated. All identified mutations in each group were first combined together in a set, then sorted on the basis of categories indicated on the top.

(C) Schematic showing specific DNA repair pathways and genes that primarily function in these pathways. The major types of DNA damage caused by mutagenic agents used in this study are shown on top and the pathways (and genes) for dealing with them shown at the bottom of the DNA schematic.

(D) Dilution spotting of S and P cells after treatment with: sodium nitrite (Nitrite), ultraviolet light (UV), hydrogen peroxide (H_2O_2), and bleomycin (Ble).

(E) Comparison of cell growth (OD_{600}) in the presence (T, treated) or absence (U, untreated) of indicated stresses. Blue: S, red: P. FD: mean fold-decrease in growth in T calculated as FD= log(T/U). [**$p < 0.01$, paired t-tests].

529 (F) Rif^{50} MF of S cells measured as in Figure 1E. WT S cells were transformed with clones of the
530 indicated DNA repair genes and changes in MF monitored. $**p < 0.01$, $***p < 0.001$; Mann-
531 Whitney test.

532 (G) Fold changes (FC) in Nitrite and Peroxide levels in P and S cells, measured using commercial
533 kits. Only peroxide levels were different. *katE, sodB* and *katG* genes were overexpressed in S cells
534 to monitor changes in these levels. $**p < 0.01$, $***p < 0.001$; Wilcoxon rank-sum test.

535

536 **Figure 3. A Global Regulatory Connection Between Efflux and DNA Repair**

537 (A) Flowchart summarizing the network analysis performed in this study.

538 (B) Scatterplots showing expression of different gene-pairs within the network that connect efflux
539 genes with DNA repair genes (color-coded as the gene-pairs in (C)); significant fold changes (±
540 1.5) are shown in matching colors with (C).
541
542 (C) Bottom: Boxplot showing distribution of significant changes color-coded in B; R is one of 100
543 randomized pairs (see Figure S3A). Top: Lines indicating the calculated Pearson correlation
544 coefficients (CC) of the corresponding pairs at the bottom. CC_S, selected pair; CC_R, random pair.

545 (D) Top: Connection of 2nd level regulatory network of DNA repair genes *mutS*, *mutM* and *ung* to
546 efflux genes, selected from the 1st level whole network (from database A in Figure 3A). Purple:
547 terminal nodes; Grey: connecting nodes. Bottom: Validated portion of network from Top, with
548 genetic connections between efflux (cyan) and DNA repair (red) genes. The connectors are efflux
549 regulators (navy), major regulators of repair genes (orange), and genes connecting regulators with
550 DNA repair (yellow). Dashed blue lines indicate an effect of efflux activity on regulators.
551 Flatheads, downregulation; Arrows, upregulation.

552 (E) Rif^{50} MF analysis of P (red) and S (blue) cells. X axis lists genetic background of S cells. [$*p$
553 < 0.05, $**p < 0.01$, $***p < 0.001$; Mann-Whitney test]

554

555 **Figure 4. The Efflux-DNA Repair Network is Clinically Relevant to the Rise in Antibiotic**
556 **Resistance**

557 (A) Flowchart summarizing the analysis of the *E. coli* antibiotic resistome data from CARD.

558 (B-F) Results from the analysis in (A). (B) Frequency distributions of mutations per genome in
559 efflux and non-efflux genomes. (C-F) Scatter plots of total number of mutations in a given genome
560 X vs number of ARMs in a specific category of genes (indicated on top) in that genome. One
561 category from each parent GO (Gene Ontology) class was taken for comparison (see Figure S4A-
562 B for details).

563 (G) Bubble matrix of calculated Spearman correlation coefficients using the data in Figure 4C-F.
564 T: total; E: Efflux; M: metabolism; R: regulatory; and C: cytosolic.

565

566 **Figure 5. The Mutator Phenotype of Swarms Can be Inhibited by Efflux Pump Inhibitors**

567 (A) Top; experimental design of MF analysis. Bottom; Kan^{50} MF of S (blue) and P (red) treated
568 (+) or untreated (-) with AcrA. [*$p < 0.05$, ***$p < 0.001$, Mann-Whitney test]

569 (B) Potential efflux pump inhibitors.

570 (C) Interaction of inhibitors in B with AcrA (PDB:2F1M). Green: Novobiocin, yellow:
571 Clorobiocin, Red: NSC60339.

572 (D) Rif^{50} MFs of WT and Δ*acrA* strains (S cells) with or without the $gyrB^{R136L}$ allele in the presence
573 of necrosignal AcrA and indicated inhibitors. -, no additions; Nov, Novobiocin; Clo, Clorobiocin;
574 NSC, NSC60339; A, purified AcrA. *$p < 0.05$, **$p < 0.01$, ***$p < 0.001$, ****$p < 0.0001$; Mann-
575 Whitney test.

576 (E) Schematic summarizing the results in D.

577

578 **Figure 6. A Role for Efflux in Iron Acquisition: Spatial Heterogeneity in Efflux, Redox, and**
579 **Cell Death**

580 (A-C) Measurement of iron in swarm cells. (A) Positioning of a swarm plate on a X-Y axis with -
581 45 to 45 mm on each direction from center. Cells from three separate regions were collected, (S_C:
582 center, S_M: middle, S_E: edge, B: blank reagent). (B) Siderophore (blue tubes in A, O-CAS assay)
583 and (C) Iron concentration (magenta tubes in A, ferrozine assay) measurements at the edge and
584 center normalized to the mean of center values. In the circular bubble-plot along the X-Y axis of
585 the plate, each bubble represents one replicate at the indicated locations on the plate. Bubble size
586 and color corresponds to the measured fold-change and color intensity in the assays.

587 (D) Quantification of roGFP intensities in S (n=1026) and P (n=792) cells (see Figure 6E, and
588 Figure S6A for S and P cell data); ****$p < 0.0001$; Wilcoxon rank-sum test.

589 (E-G) roGFP fluorescence images (top) and frequency distribution (bottom) of S cells collected
590 from the entire swarm plate. (E) Two populations of fluorescence intensities are observed (AU,
591 arbitrary units) (see Figure S6 C-E for brightfield images). (F, G) as in E except S cells were taken
592 from either the center or the edge.

593 (H-J) roGFP-efflux correlation in S cells. (H) From left to right: bright field, roGFP, Nile red dye.
594 (I) Distribution of Nile red fluorescence. (J) Anti-correlation of Nile red and roGFP (n=202); R^2=
595 0.5919.

596 (K-M) roGFP-CTC correlation in S cells. (K) From left to right: bright field, roGFP, CTC (false
597 colored blue). (L) Distribution of CTC fluorescence. (M) Correlation of CTC and roGFP (n=51);
598 R^2= 0.5012.

599 (N) Live-Dead staining of P (left) and S (right) cells showing superimposed live (SYTO9) and
600 dead (PI) stains (see Figure S6I for brightfield images).

601 (O) Percentage of dead cells. P_S, P stationary; P_L, P log phase; S_C and S_E, S cells from center and
602 edge of swarm. [t-tests performed by comparing each S set to P_S, **$p < 0.01$, ***$p < 0.001$, ****p
603 < 0.0001]

604

605 **Figure 7. Phenotype Surfing: an Evolutionary Mechanism for Breeding Mutants that**
606 **Survive in the Absence of Selection**

607 (A) A 3D plot of experimentally derived values of growth rate (G, in generations per hour, x-axis),
608 mutation frequency (MF in 10^{-7}/CFU, y-axis), and evolvability (E, Z-axis). Arrows indicate
609 direction of change.

610 (B) Rif^{50} MF of S cells sampled from different regions. S refers to entire population.

611 (C) Swim motility assays with cells collected from swarm plates (see Figure S7G for images).

612 (D) Phenotypic surfing model. Top: a side view of a swarm population with the distribution of two
613 phenotypically distinct cell types (orange and blue) in a spatially segregated edge zone. In this
614 example, the edge has reached an antibiotic zone (olive). Blue cells are more motile and efflux
615 more, producing mutants (red and black) some of which die (black) in absence of a favorable
616 environment. The blue cells and their red progeny 'surf' at the edge of the colony either by a faster
617 migration to the edge (dashed arrows) or are favored at the edge to bring in iron. Bottom: Summary
618 of mechanism underlying the phenotypic differences between orange and blue cells. The yellow-
619 red gauge indicates ROS levels, which are high in blue cells. A series of network interactions
620 starting from efflux nodes (blue), through stress (red), and other intermediate nodes (Inter, yellow)
621 decrease DNA repair activity (teal) in blue cells, increasing mutations (red).

622 (D-E) $*p < 0.05$, $***p < 0.001$; Mann-Whitney test.

623

624 **SUPPLEMENTAL INFORMATION**

625 The supplementary information file contains Materials and Methods, Supplementary Text,
626 Supplementary Videos, Figures S1 to S7, Table S1, and References

627

628

629 **REFERENCES**

630 Abdali, N., Parks, J.M., Haynes, K.M., Chaney, J.L., Green, A.T., Wolloscheck, D., Walker, J.K., Rybenkov,
631 V.V., Baudry, J., Smith, J.C., *et al.* (2017). Reviving Antibiotics: Efflux Pump Inhibitors That Interact with
632 AcrA, a Membrane Fusion Protein of the AcrAB-TolC Multidrug Efflux Pump. ACS infectious diseases *3*,
633 89-98.
634 Alav, I., Sutton, J.M., and Rahman, K.M. (2018). Role of bacterial efflux pumps in biofilm formation. The
635 Journal of antimicrobial chemotherapy *73*, 2003-2020.
636 Alcock, B.P., Raphenya, A.R., Lau, T.T.Y., Tsang, K.K., Bouchard, M., Edalatmand, A., Huynh, W., Nguyen,
637 A.V., Cheng, A.A., Liu, S., *et al.* (2020). CARD 2020: antibiotic resistome surveillance with the
638 comprehensive antibiotic resistance database. Nucleic acids research *48*, D517-D525.
639 Allison, K.R., Brynildsen, M.P., and Collins, J.J. (2011). Metabolite-enabled eradication of bacterial
640 persisters by aminoglycosides. Nature *473*, 216-220.

641 Andersson, D.I., and Levin, B.R. (1999). The biological cost of antibiotic resistance. Current opinion in
642 microbiology *2*, 489-493.
643 Anes, J., McCusker, M.P., Fanning, S., and Martins, M. (2015). The ins and outs of RND efflux pumps in
644 Escherichia coli. Frontiers in microbiology *6*, 587.
645 Becker, B., and Cooper, M.A. (2013). Aminoglycoside antibiotics in the 21st century. ACS chemical
646 biology *8*, 105-115.
647 Bhattacharyya, S., Walker, D.M., and Harshey, R.M. (2020). Dead cells release a 'necrosignal' that
648 activates antibiotic survival pathways in bacterial swarms. Nature communications *11*, 4157.
649 Bjorkman, J., Nagaev, I., Berg, O.G., Hughes, D., and Andersson, D.I. (2000). Effects of environment on
650 compensatory mutations to ameliorate costs of antibiotic resistance. Science *287*, 1479-1482.
651 Bleuel, C., Grosse, C., Taudte, N., Scherer, J., Wesenberg, D., Krauss, G.J., Nies, D.H., and Grass, G.
652 (2005). TolC is involved in enterobactin efflux across the outer membrane of Escherichia coli. Journal of
653 bacteriology *187*, 6701-6707.
654 Bohnert, J.A., Karamian, B., and Nikaido, H. (2010). Optimized Nile Red efflux assay of AcrAB-TolC
655 multidrug efflux system shows competition between substrates. Antimicrobial agents and
656 chemotherapy *54*, 3770-3775.
657 Bottger, E.C., Pletschette, M., and Andersson, D. (2005). Drug resistance and fitness in Mycobacterium
658 tuberculosis infection. The Journal of infectious diseases *191*, 823-824; author reply 824.
659 Brauner, A., Fridman, O., Gefen, O., and Balaban, N.Q. (2016). Distinguishing between resistance,
660 tolerance and persistence to antibiotic treatment. Nature reviews Microbiology *14*, 320-330.
661 Butler, M.T., Wang, Q., and Harshey, R.M. (2010). Cell density and mobility protect swarming bacteria
662 against antibiotics. Proceedings of the National Academy of Sciences of the United States of America
663 *107*, 3776-3781.
664 Chang, D.E., Smalley, D.J., and Conway, T. (2002). Gene expression profiling of Escherichia coli growth
665 transitions: an expanded stringent response model. Molecular microbiology *45*, 289-306.
666 Chevance, F.F., and Hughes, K.T. (2008). Coordinating assembly of a bacterial macromolecular machine.
667 Nature reviews Microbiology *6*, 455-465.
668 Connell, S.R., Takemoto, C., Wilson, D.N., Wang, H., Murayama, K., Terada, T., Shirouzu, M., Rost, M.,
669 Schuler, M., Giesebrecht, J.*, et al.* (2007). Structural basis for interaction of the ribosome with the switch
670 regions of GTP-bound elongation factors. Molecular cell *25*, 751-764.
671 Davies, B.W., Bogard, R.W., Dupes, N.M., Gerstenfeld, T.A., Simmons, L.A., and Mekalanos, J.J. (2011).
672 DNA damage and reactive nitrogen species are barriers to Vibrio cholerae colonization of the infant
673 mouse intestine. PLoS pathogens *7*, e1001295.
674 Du, D., Wang-Kan, X., Neuberger, A., van Veen, H.W., Pos, K.M., Piddock, L.J.V., and Luisi, B.F. (2018).
675 Multidrug efflux pumps: structure, function and regulation. Nature reviews Microbiology *16*, 523-539.
676 Du Toit, A. (2017). Bacterial physiology: Efflux pumps, fitness and virulence. Nature reviews
677 Microbiology *15*, 512-513.
678 Dukan, S., and Nystrom, T. (1998). Bacterial senescence: stasis results in increased and differential
679 oxidation of cytoplasmic proteins leading to developmental induction of the heat shock regulon. Genes
680 & development *12*, 3431-3441.
681 Dwyer, D.J., Belenky, P.A., Yang, J.H., MacDonald, I.C., Martell, J.D., Takahashi, N., Chan, C.T., Lobritz,
682 M.A., Braff, D., Schwarz, E.G.*, et al.* (2014). Antibiotics induce redox-related physiological alterations as
683 part of their lethality. Proceedings of the National Academy of Sciences of the United States of America
684 *111*, E2100-2109.
685 El Meouche, I., and Dunlop, M.J. (2018). Heterogeneity in efflux pump expression predisposes antibiotic-
686 resistant cells to mutation. Science *362*, 686-690.
687 Elena, S.F., and Lenski, R.E. (2003). Evolution experiments with microorganisms: the dynamics and
688 genetic bases of adaptation. Nature reviews Genetics *4*, 457-469.

689 Fang, F.C. (2011). Antimicrobial actions of reactive oxygen species. mBio *2*.
690 Fitzgerald, D.M., Hastings, P.J., and Rosenberg, S.M. (2017). Stress-Induced Mutagenesis: Implications in
691 Cancer and Drug Resistance. Annual review of cancer biology *1*, 119-140.
692 Flemming, H.C., Wingender, J., Szewzyk, U., Steinberg, P., Rice, S.A., and Kjelleberg, S. (2016). Biofilms:
693 an emergent form of bacterial life. Nature reviews Microbiology *14*, 563-575.
694 Fowler, R.G., Erickson, J.A., and Isbell, R.J. (1994). Activity of the Escherichia coli mutT mutator allele in
695 an anaerobic environment. Journal of bacteriology *176*, 7727-7729.
696 Friedberg, E.C.F.E.C. (2006). DNA repair and mutagenesis (Washington, D.C.: ASM Press).
697 Gabel, C.V., and Berg, H.C. (2003). The speed of the flagellar rotary motor of Escherichia coli varies
698 linearly with protonmotive force. Proceedings of the National Academy of Sciences of the United States
699 of America *100*, 8748-8751.
700 Grainger, D.C., Hurd, D., Harrison, M., Holdstock, J., and Busby, S.J. (2005). Studies of the distribution of
701 Escherichia coli cAMP-receptor protein and RNA polymerase along the E. coli chromosome. Proceedings
702 of the National Academy of Sciences of the United States of America *102*, 17693-17698.
703 Gross, C.H., Parsons, J.D., Grossman, T.H., Charifson, P.S., Bellon, S., Jernee, J., Dwyer, M., Chambers,
704 S.P., Markland, W., Botfield, M.*, et al.* (2003). Active-site residues of Escherichia coli DNA gyrase
705 required in coupling ATP hydrolysis to DNA supercoiling and amino acid substitutions leading to
706 novobiocin resistance. Antimicrobial agents and chemotherapy *47*, 1037-1046.
707 Hallatschek, O., and Nelson, D.R. (2008). Gene surfing in expanding populations. Theoretical population
708 biology *73*, 158-170.
709 Harshey, R.M. (2003). Bacterial motility on a surface: many ways to a common goal. Annual review of
710 microbiology *57*, 249-273.
711 Henderson, P.J.F., Maher, C., Elbourne, L.D.H., Eijkelkamp, B.A., Paulsen, I.T., and Hassan, K.A. (2021).
712 Physiological Functions of Bacterial "Multidrug" Efflux Pumps. Chemical reviews *121*, 5417-5478.
713 Hengge, R. (2009). Principles of c-di-GMP signalling in bacteria. Nature reviews Microbiology *7*, 263-273.
714 Hibbing, M.E., Fuqua, C., Parsek, M.R., and Peterson, S.B. (2010). Bacterial competition: surviving and
715 thriving in the microbial jungle. Nature reviews Microbiology *8*, 15-25.
716 Hoiby, N., Bjarnsholt, T., Givskov, M., Molin, S., and Ciofu, O. (2010). Antibiotic resistance of bacterial
717 biofilms. International journal of antimicrobial agents *35*, 322-332.
718 Hol, F.J., Hubert, B., Dekker, C., and Keymer, J.E. (2016). Density-dependent adaptive resistance allows
719 swimming bacteria to colonize an antibiotic gradient. The ISME journal *10*, 30-38.
720 Husemann, M., Zachos, F.E., Paxton, R.J., and Habel, J.C. (2016). Effective population size in ecology and
721 evolution. Heredity *117*, 191-192.
722 Imlay, J.A. (2013). The molecular mechanisms and physiological consequences of oxidative stress:
723 lessons from a model bacterium. Nature reviews Microbiology *11*, 443-454.
724 Inoue, T., Shingaki, R., Hirose, S., Waki, K., Mori, H., and Fukui, K. (2007). Genome-wide screening of
725 genes required for swarming motility in Escherichia coli K-12. Journal of bacteriology *189*, 950-957.
726 Ishihama, A., Shimada, T., and Yamazaki, Y. (2016). Transcription profile of Escherichia coli: genomic
727 SELEX search for regulatory targets of transcription factors. Nucleic acids research *44*, 2058-2074.
728 Jenal, U., Reinders, A., and Lori, C. (2017). Cyclic di-GMP: second messenger extraordinaire. Nature
729 reviews Microbiology *15*, 271-284.
730 Kapoor, I., Emam, E.A.F., Shaw, A., and Varshney, U. (2019). Nucleoside Diphosphate Kinase Escalates A-
731 to-C Mutations in MutT-Deficient Strains of Escherichia coli. Journal of bacteriology *202*.
732 Kearns, D.B. (2010). A field guide to bacterial swarming motility. Nature reviews Microbiology *8*, 634-
733 644.
734 Keseler, I.M., Collado-Vides, J., Santos-Zavaleta, A., Peralta-Gil, M., Gama-Castro, S., Muniz-Rascado, L.,
735 Bonavides-Martinez, C., Paley, S., Krummenacker, M., Altman, T.*, et al.* (2011). EcoCyc: a comprehensive
736 database of Escherichia coli biology. Nucleic acids research *39*, D583-590.

737 Kim, W., Killam, T., Sood, V., and Surette, M.G. (2003). Swarm-cell differentiation in Salmonella enterica
738 serovar typhimurium results in elevated resistance to multiple antibiotics. Journal of bacteriology *185*,
739 3111-3117.
740 Kohanski, M.A., Dwyer, D.J., and Collins, J.J. (2010). How antibiotics kill bacteria: from targets to
741 networks. Nature reviews Microbiology *8*, 423-435.
742 Kramer, J., Ozkaya, O., and Kummerli, R. (2020). Bacterial siderophores in community and host
743 interactions. Nature reviews Microbiology *18*, 152-163.
744 Krasovec, R., Belavkin, R.V., Aston, J.A., Channon, A., Aston, E., Rash, B.M., Kadirvel, M., Forbes, S., and
745 Knight, C.G. (2014). Mutation rate plasticity in rifampicin resistance depends on Escherichia coli cell-cell
746 interactions. Nature communications *5*, 3742.
747 Krasovec, R., Richards, H., Gifford, D.R., Hatcher, C., Faulkner, K.J., Belavkin, R.V., Channon, A., Aston, E.,
748 McBain, A.J., and Knight, C.G. (2017). Spontaneous mutation rate is a plastic trait associated with
749 population density across domains of life. PLoS biology *15*, e2002731.
750 Kurthkoti, K., Kumar, P., Jain, R., and Varshney, U. (2008). Important role of the nucleotide excision
751 repair pathway in Mycobacterium smegmatis in conferring protection against commonly encountered
752 DNA-damaging agents. Microbiology *154*, 2776-2785.
753 Lai, S., Tremblay, J., and Deziel, E. (2009). Swarming motility: a multicellular behaviour conferring
754 antimicrobial resistance. Environmental microbiology *11*, 126-136.
755 Laland, K.N., Sterelny, K., Odling-Smee, J., Hoppitt, W., and Uller, T. (2011). Cause and effect in biology
756 revisited: is Mayr's proximate-ultimate dichotomy still useful? Science *334*, 1512-1516.
757 Landini, P., Egli, T., Wolf, J., and Lacour, S. (2014). sigmaS, a major player in the response to
758 environmental stresses in Escherichia coli: role, regulation and mechanisms of promoter recognition.
759 Environmental microbiology reports *6*, 1-13.
760 Larkin, J.W., Zhai, X., Kikuchi, K., Redford, S.E., Prindle, A., Liu, J., Greenfield, S., Walczak, A.M., Garcia-
761 Ojalvo, J., Mugler, A.*, et al.* (2018). Signal Percolation within a Bacterial Community. Cell systems *7*, 137-
762 145 e133.
763 Li, X.Z., Plesiat, P., and Nikaido, H. (2015). The challenge of efflux-mediated antibiotic resistance in
764 Gram-negative bacteria. Clinical microbiology reviews *28*, 337-418.
765 Libby, E., and Rainey, P.B. (2011). Exclusion rules, bottlenecks and the evolution of stochastic phenotype
766 switching. Proceedings Biological sciences *278*, 3574-3583.
767 Lin, C.S., Tsai, Y.H., Chang, C.J., Tseng, S.F., Wu, T.R., Lu, C.C., Wu, T.S., Lu, J.J., Horng, J.T., Martel, J.*, et*
768 *al.* (2016). An iron detection system determines bacterial swarming initiation and biofilm formation.
769 Scientific reports *6*, 36747.
770 Lynch, M., Ackerman, M.S., Gout, J.F., Long, H., Sung, W., Thomas, W.K., and Foster, P.L. (2016). Genetic
771 drift, selection and the evolution of the mutation rate. Nature reviews Genetics *17*, 704-714.
772 MacLean, R.C., Torres-Barcelo, C., and Moxon, R. (2013). Evaluating evolutionary models of stress-
773 induced mutagenesis in bacteria. Nature reviews Genetics *14*, 221-227.
774 Mahoney, A.R., Safaee, M.M., Wuest, W.M., and Furst, A.L. (2021). The silent pandemic: Emergent
775 antibiotic resistances following the global response to SARS-CoV-2. iScience *24*, 102304.
776 Mayr, E. (1961). Cause and effect in biology. Science *134*, 1501-1506.
777 McCarter, L., and Silverman, M. (1989). Iron regulation of swarmer cell differentiation of Vibrio
778 parahaemolyticus. Journal of bacteriology *171*, 731-736.
779 Melnyk, A.H., Wong, A., and Kassen, R. (2015). The fitness costs of antibiotic resistance mutations.
780 Evolutionary applications *8*, 273-283.
781 Mendelson, M., Sharland, M., and Mpundu, M. (2022). Antibiotic resistance: calling time on the 'silent
782 pandemic'. JAC-antimicrobial resistance *4*, dlac016.

783 Milanowska, K., Krwawicz, J., Papaj, G., Kosinski, J., Poleszak, K., Lesiak, J., Osinska, E., Rother, K., and
784 Bujnicki, J.M. (2011). REPAIRtoire--a database of DNA repair pathways. Nucleic acids research *39*, D788-
785 792.
786 Miller, J.H., Ganem, D., Lu, P., and Schmitz, A. (1977). Genetic studies of the lac repressor. I. Correlation
787 of mutational sites with specific amino acid residues: construction of a colinear gene-protein map.
788 Journal of molecular biology *109*, 275-298.
789 Moretto, M., Sonego, P., Dierckxsens, N., Brilli, M., Bianco, L., Ledezma-Tejeida, D., Gama-Castro, S.,
790 Galardini, M., Romualdi, C., Laukens, K.*, et al.* (2016). COLOMBOS v3.0: leveraging gene expression
791 compendia for cross-species analyses. Nucleic acids research *44*, D620-623.
792 Morgan, B., Sobotta, M.C., and Dick, T.P. (2011). Measuring E(GSH) and H2O2 with roGFP2-based redox
793 probes. Free radical biology & medicine *51*, 1943-1951.
794 Nikaido, H., and Pages, J.M. (2012). Broad-specificity efflux pumps and their role in multidrug resistance
795 of Gram-negative bacteria. FEMS microbiology reviews *36*, 340-363.
796 Nishino, K., Nikaido, E., and Yamaguchi, A. (2009). Regulation and physiological function of multidrug
797 efflux pumps in Escherichia coli and Salmonella. Biochimica et biophysica acta *1794*, 834-843.
798 Otto, S.P., and Whitlock, M.C. (1997). The probability of fixation in populations of changing size.
799 Genetics *146*, 723-733.
800 Oviedo, C., Contreras, D., Freer, J., and Rodriguez, J. (2003). A screening method for detecting iron
801 reducing wood-rot fungi. Biotechnology letters *25*, 891-893.
802 Partridge, J.D., and Harshey, R.M. (2013a). More than motility: Salmonella flagella contribute to
803 overriding friction and facilitating colony hydration during swarming. Journal of bacteriology *195*, 919-
804 929.
805 Partridge, J.D., and Harshey, R.M. (2013b). Swarming: flexible roaming plans. Journal of bacteriology
806 *195*, 909-918.
807 Payne, J.L., and Wagner, A. (2019). The causes of evolvability and their evolution. Nature reviews
808 Genetics *20*, 24-38.
809 Pesavento, C., Becker, G., Sommerfeldt, N., Possling, A., Tschowri, N., Mehlis, A., and Hengge, R. (2008).
810 Inverse regulatory coordination of motility and curli-mediated adhesion in Escherichia coli. Genes &
811 development *22*, 2434-2446.
812 Pigliucci, M. (2008). Is evolvability evolvable? Nature reviews Genetics *9*, 75-82.
813 Ram, Y., and Hadany, L. (2014). Stress-induced mutagenesis and complex adaptation. Proceedings
814 Biological sciences *281*.
815 Rodriguez, G.G., Phipps, D., Ishiguro, K., and Ridgway, H.F. (1992). Use of a fluorescent redox probe for
816 direct visualization of actively respiring bacteria. Applied and environmental microbiology *58*, 1801-
817 1808.
818 Rosenberg, S.M., Shee, C., Frisch, R.L., and Hastings, P.J. (2012). Stress-induced mutation via DNA breaks
819 in Escherichia coli: a molecular mechanism with implications for evolution and medicine. BioEssays :
820 news and reviews in molecular, cellular and developmental biology *34*, 885-892.
821 Rosner, J.L., and Martin, R.G. (2013). Reduction of cellular stress by TolC-dependent efflux pumps in
822 Escherichia coli indicated by BaeSR and CpxARP activation of spy in efflux mutants. Journal of
823 bacteriology *195*, 1042-1050.
824 Schwyn, B., and Neilands, J.B. (1987). Universal chemical assay for the detection and determination of
825 siderophores. Analytical biochemistry *160*, 47-56.
826 Shallcross, L., Beckley, N., Rait, G., Hayward, A., and Petersen, I. (2017). Antibiotic prescribing frequency
827 amongst patients in primary care: a cohort study using electronic health records. The Journal of
828 antimicrobial chemotherapy *72*, 1818-1824.
829 Sousa, A., Magalhaes, S., and Gordo, I. (2012). Cost of antibiotic resistance and the geometry of
830 adaptation. Molecular biology and evolution *29*, 1417-1428.

831 Sprouffske, K., Aguilar-Rodriguez, J., Sniegowski, P., and Wagner, A. (2018). High mutation rates limit
832 evolutionary adaptation in Escherichia coli. PLoS genetics *14*, e1007324.
833 Steenackers, H.P., Parijs, I., Dubey, A., Foster, K.R., and Vanderleyden, J. (2016). Experimental evolution
834 in biofilm populations. FEMS microbiology reviews *40*, 373-397.
835 Sun, J., Deng, Z., and Yan, A. (2014). Bacterial multidrug efflux pumps: mechanisms, physiology and
836 pharmacological exploitations. Biochemical and biophysical research communications *453*, 254-267.
837 Traxler, M.F., and Kolter, R. (2015). Natural products in soil microbe interactions and evolution. Natural
838 product reports *32*, 956-970.
839 van der Heijden, J., Vogt, S.L., Reynolds, L.A., Pena-Diaz, J., Tupin, A., Aussel, L., and Finlay, B.B. (2016).
840 Exploring the redox balance inside gram-negative bacteria with redox-sensitive GFP. Free radical biology
841 & medicine *91*, 34-44.
842 Voorhees, R.M., and Ramakrishnan, V. (2013). Structural basis of the translational elongation cycle.
843 Annual review of biochemistry *82*, 203-236.
844 Wang, Q., Frye, J.G., McClelland, M., and Harshey, R.M. (2004). Gene expression patterns during
845 swarming in Salmonella typhimurium: genes specific to surface growth and putative new motility and
846 pathogenicity genes. Molecular microbiology *52*, 169-187.
847 Webber, M.A., and Piddock, L.J. (2003). The importance of efflux pumps in bacterial antibiotic
848 resistance. The Journal of antimicrobial chemotherapy *51*, 9-11.
849 Wilson, B.R., Bogdan, A.R., Miyazawa, M., Hashimoto, K., and Tsuji, Y. (2016). Siderophores in Iron
850 Metabolism: From Mechanism to Therapy Potential. Trends in molecular medicine *22*, 1077-1090.
851 Zhou, J., Lancaster, L., Donohue, J.P., and Noller, H.F. (2014). How the ribosome hands the A-site tRNA to
852 the P site during EF-G-catalyzed translocation. Science *345*, 1188-1191.

853

Figure 1

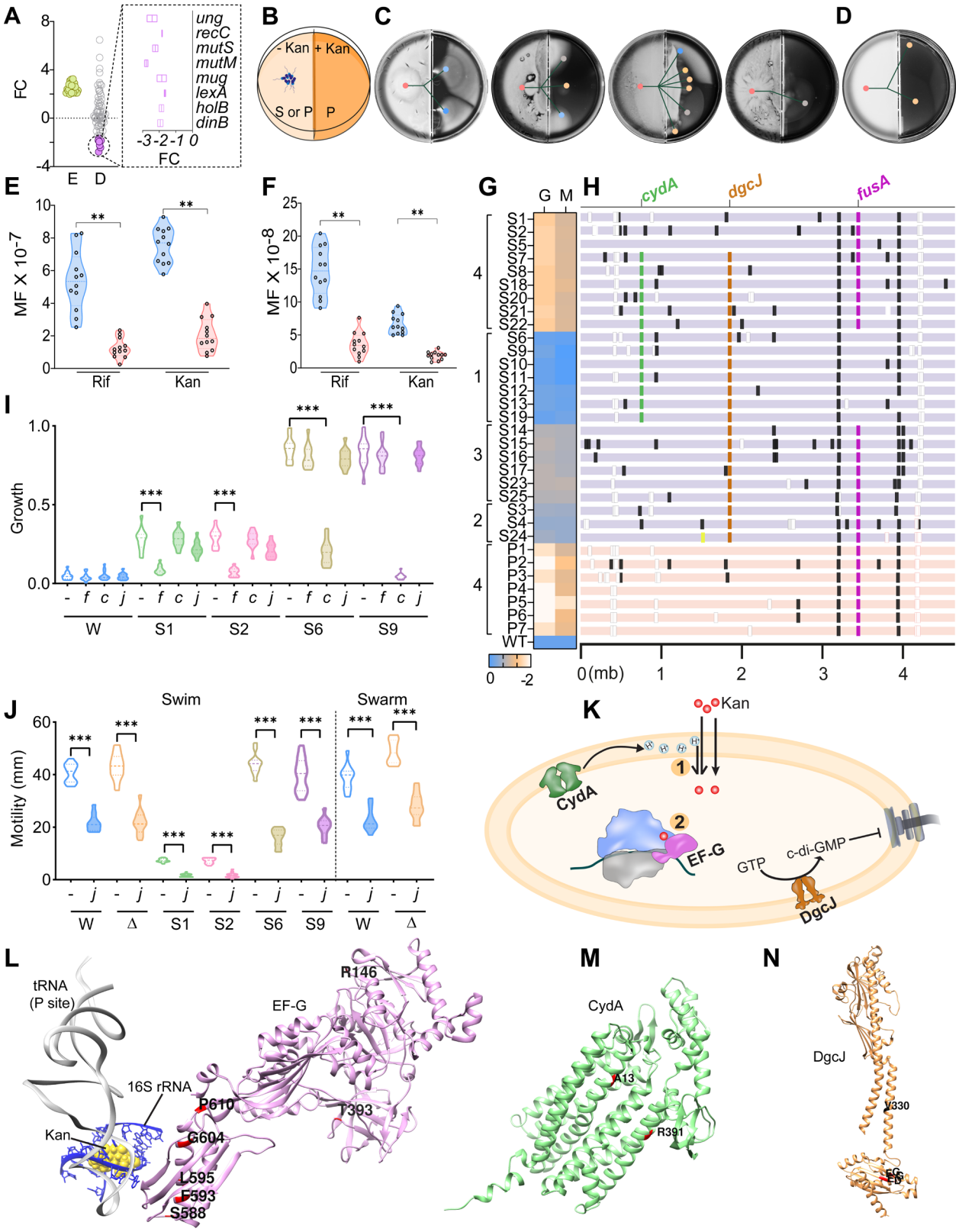
A
FC
ung
recC
mutS
mutM
mug
lexA
holB
dinB
-3 -2 -1 0
FC
E D
B
- Kan + Kan
S or P
P
C
D
E
MF X 10-7
Rif
Kan
F
MF X 10-8
Rif
Kan
G
G M
H
cydA
dgcJ
fusA
S1
S2
S5
S7
S8
S18
S20
S21
S22
S6
S9
S10
S11
S12
S13
S19
S14
S15
S16
S17
S23
S25
S3
S4
S24
P1
P2
P3
P4
P5
P6
P7
WT
0 -2
0 (mb) 1 2 3 4
I
Growth
- f c j
W S1 S2 S6 S9
J
Swim
Swarm
Motility (mm)
W Δ S1 S2 S6 S9 W Δ
K
Kan
CydA
EF-G
GTP
c-di-GMP
DgcJ
L
tRNA
(P site)
EF-G
R146
16S rRNA
P610
T393
Kan
G604
L595
F593
S588
M
CydA
A13
R391
N
DgcJ
V330

Figure 2

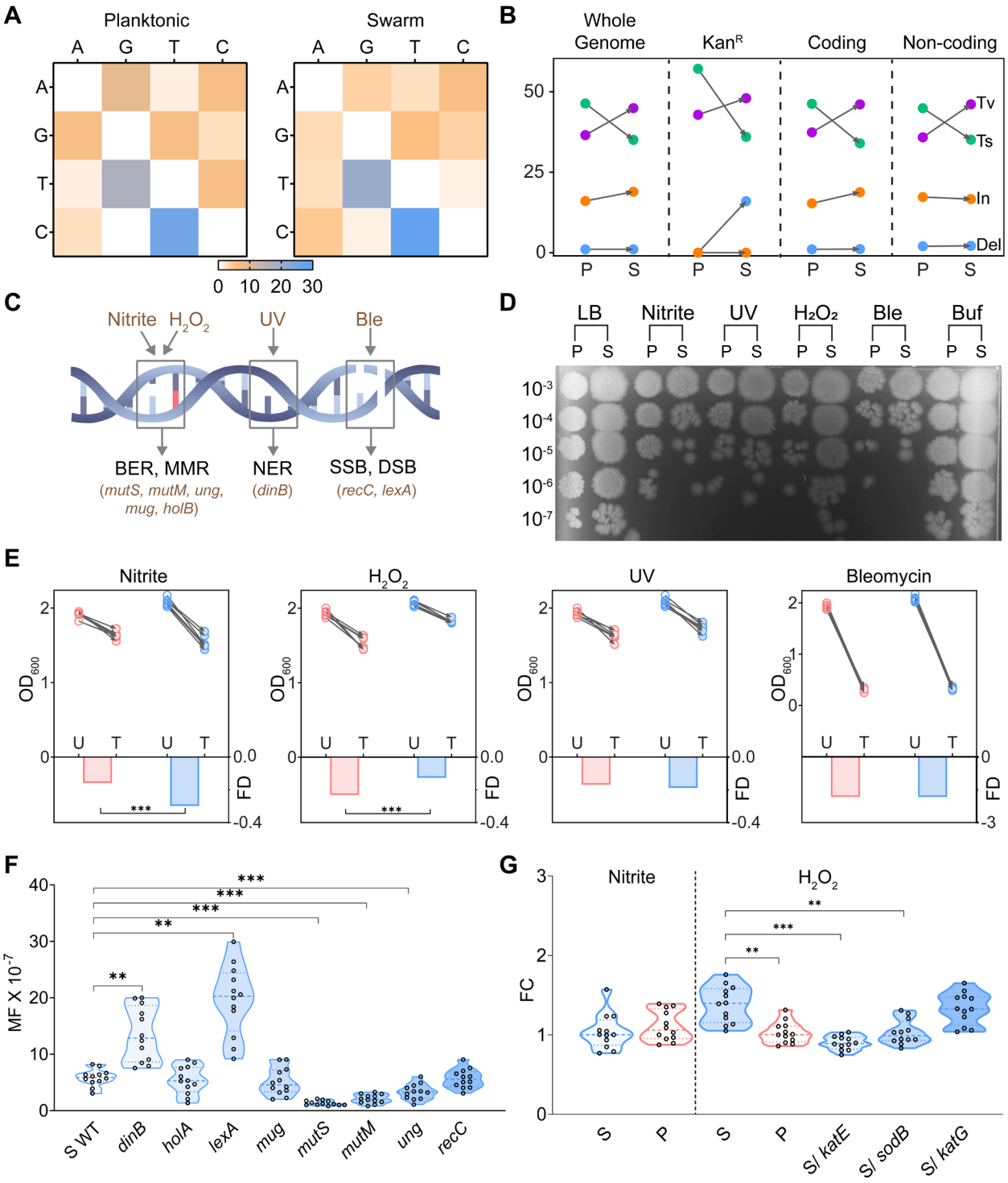
A
Planktonic
Swarm
A G T C
0 10 20 30
B
Whole Genome
KanR
Coding
Non-coding
Tv
Ts
In
Del
P S
C
Nitrite
H2O2
UV
Ble
BER, MMR
(mutS, mutM, ung, mug, holB)
NER
(dinB)
SSB, DSB
(recC, lexA)
D
LB
Nitrite
UV
H2O2
Ble
Buf
E
Nitrite
H2O2
UV
Bleomycin
OD600
FD
U T
***
F
MF X 10-7
S WT
dinB
holA
lexA
mug
mutS
mutM
ung
recC
G
Nitrite
H2O2
FC
S
P
S/ katE
S/ sodB
S/ katG

Figure 3

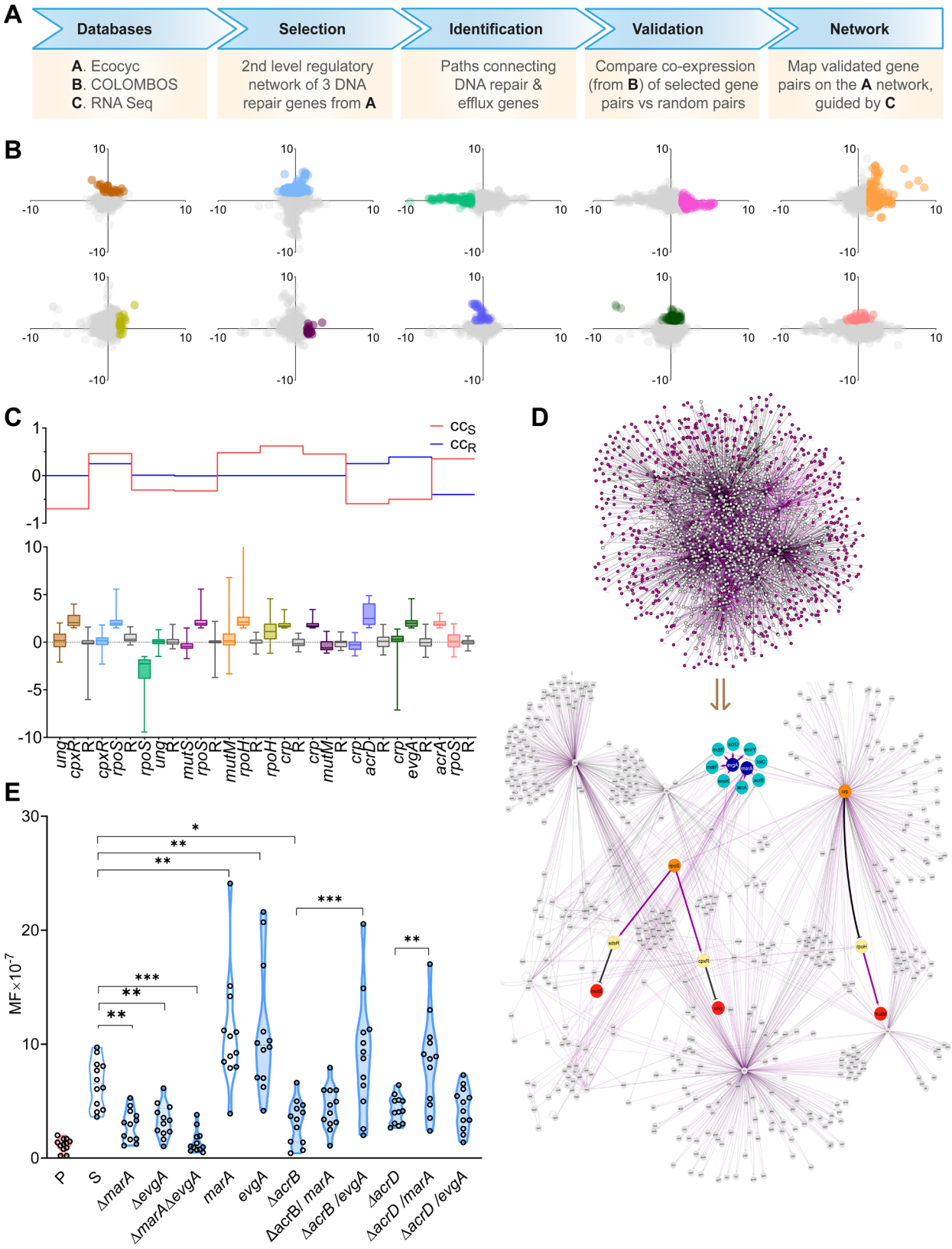
A
Databases
Selection
Identification
Validation
Network
A. Ecocyc
B. COLOMBOS
C. RNA Seq
2nd level regulatory network of 3 DNA repair genes from A
Paths connecting DNA repair & efflux genes
Compare co-expression (from B) of selected gene pairs vs random pairs
Map validated gene pairs on the A network, guided by C
B
C
CCS
CCR
D
E
MF×10-7
P
S
ΔmarA
ΔevgA
ΔmarAΔevgA
marA
evgA
ΔacrB
ΔacrB/ marA
ΔacrB /evgA
ΔacrD
ΔacrD /marA
ΔacrD /evgA

Figure 3

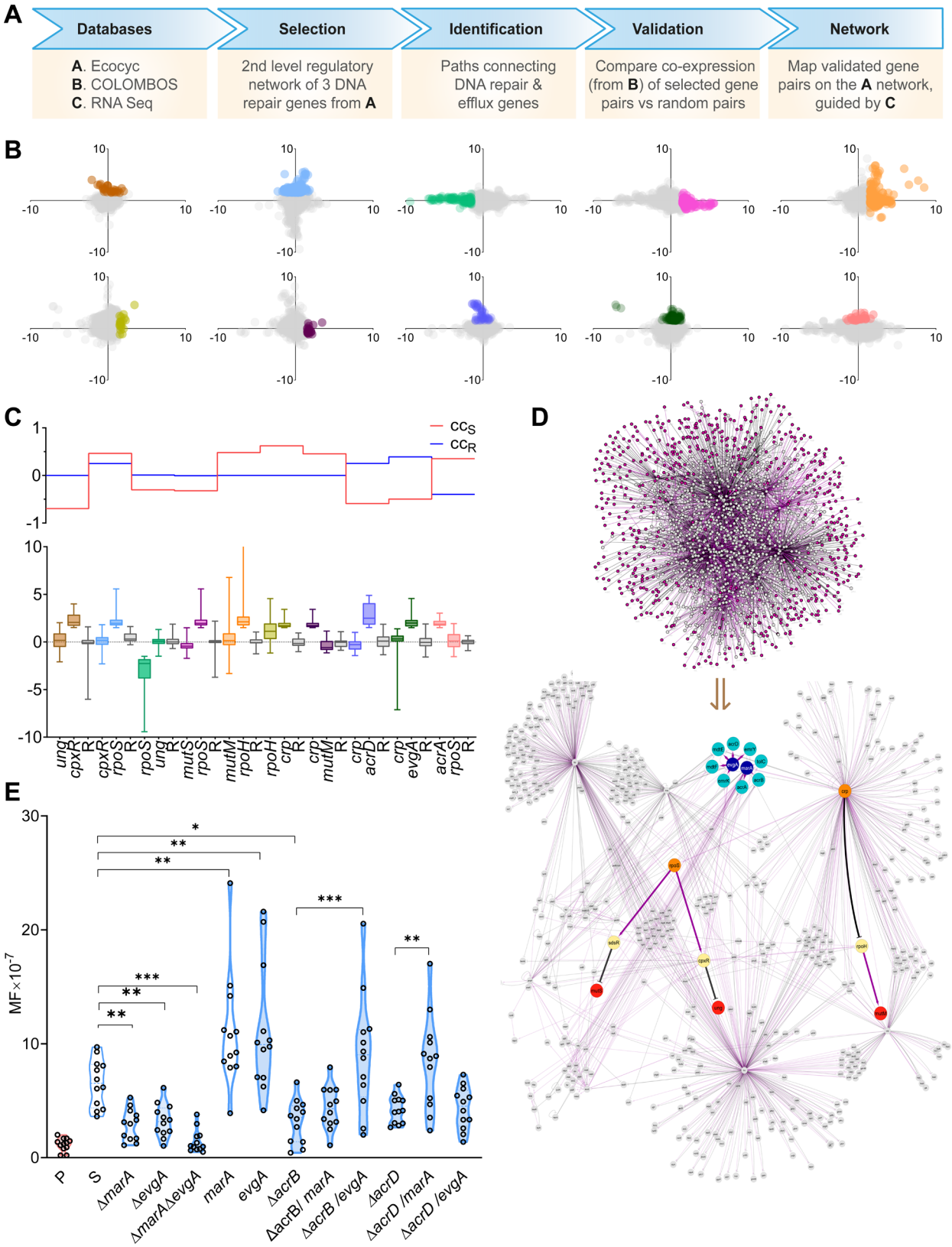
A
Databases
Selection
Identification
Validation
Network
A. Ecocyc
B. COLOMBOS
C. RNA Seq
2nd level regulatory network of 3 DNA repair genes from A
Paths connecting DNA repair & efflux genes
Compare co-expression (from B) of selected gene pairs vs random pairs
Map validated gene pairs on the A network, guided by C
B
C
CCS
CCR
D
E
MF×10-7
P
S
ΔmarA
ΔevgA
ΔmarAΔevgA
marA
evgA
ΔacrB
ΔacrB/ marA
ΔacrB /evgA
ΔacrD
ΔacrD /marA
ΔacrD /evgA

Figure 4

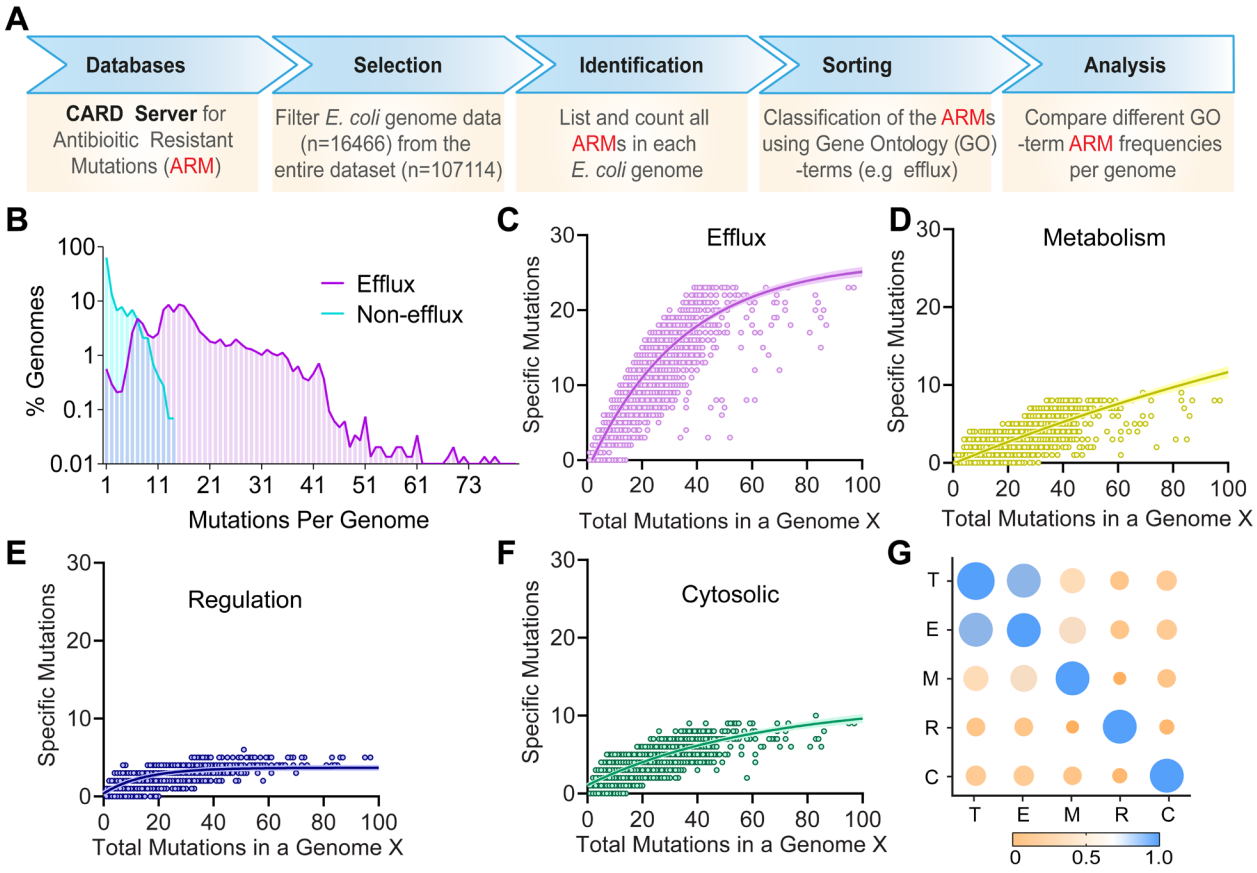
A
Databases
Selection
Identification
Sorting
Analysis
CARD Server for Antibioitic Resistant Mutations (ARM)
Filter E. coli genome data (n=16466) from the entire dataset (n=107114)
List and count all ARMs in each E. coli genome
Classification of the ARMs using Gene Ontology (GO) -terms (e.g efflux)
Compare different GO -term ARM frequencies per genome
B
% Genomes
Efflux
Non-efflux
Mutations Per Genome
C
Efflux
Specific Mutations
Total Mutations in a Genome X
D
Metabolism
Specific Mutations
Total Mutations in a Genome X
E
Regulation
Specific Mutations
Total Mutations in a Genome X
F
Cytosolic
Specific Mutations
Total Mutations in a Genome X
G
T
E
M
R
C
0
0.5
1.0

Figure 5

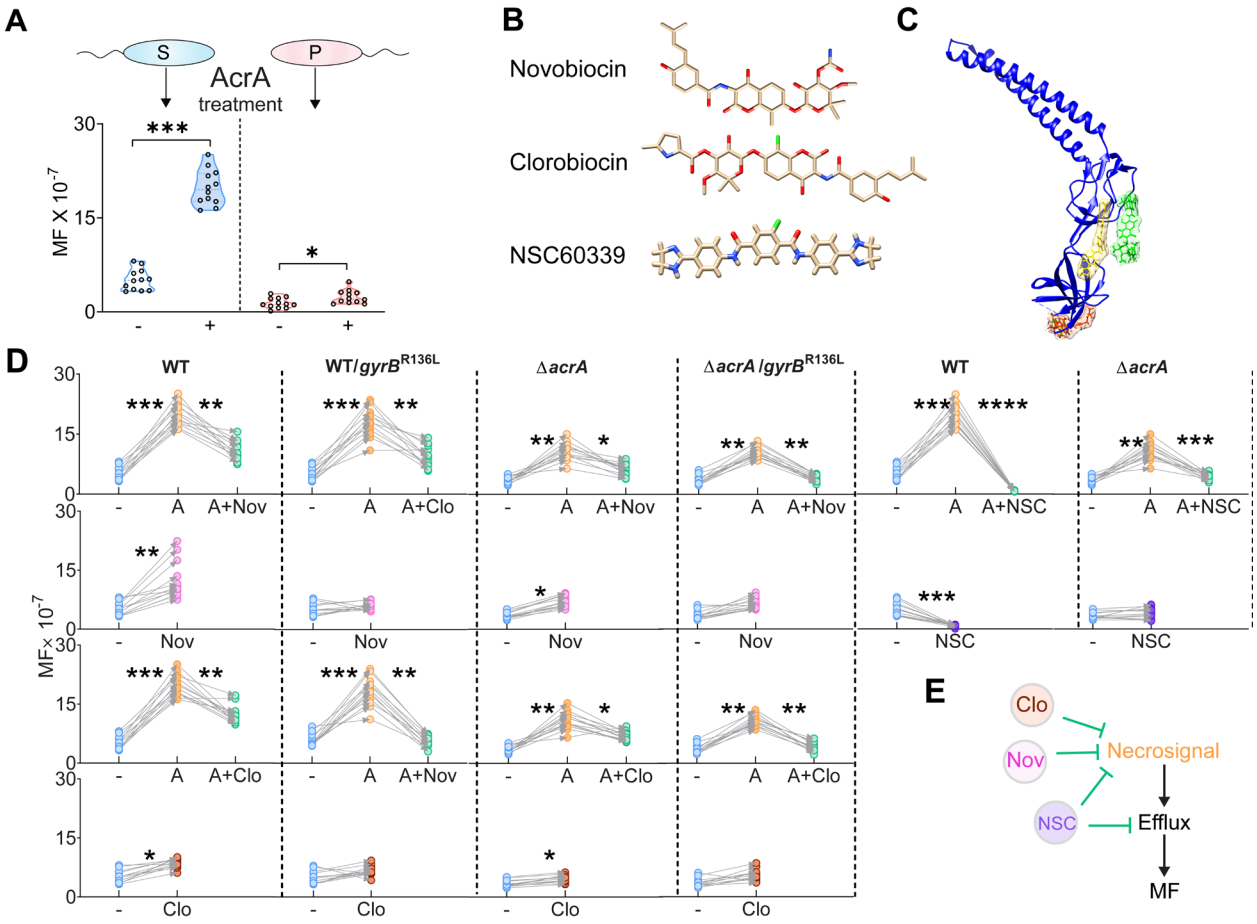
A
S
P
AcrA
treatment
MF X 10^-7
30
15
0
***
*
-
+
B
Novobiocin
Clorobiocin
NSC60339
C
D
WT
WT/gyrB^R136L
ΔacrA
ΔacrA /gyrB^R136L
WT
ΔacrA
MF× 10^-7
A
A+Nov
A+Clo
A+NSC
Nov
NSC
Clo
E
Clo
Nov
NSC
Necrosignal
Efflux
MF

Figure 6

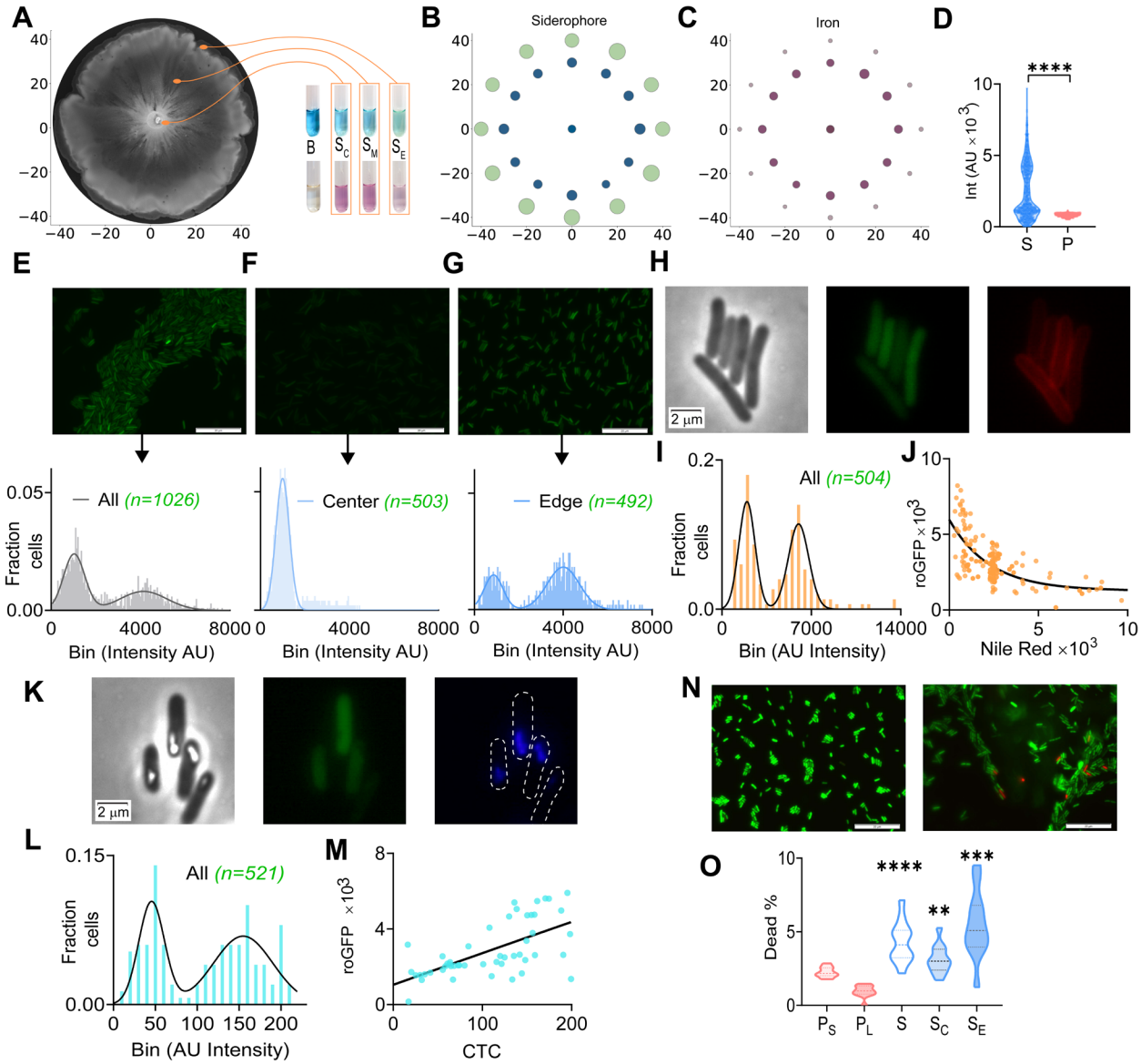
A
B
Siderophore
C
Iron
D
****
Int (AU ×10^3)
S
P
E
F
G
H
2 µm
All (n=1026)
Center (n=503)
Edge (n=492)
Fraction cells
Bin (Intensity AU)
I
All (n=504)
Bin (AU Intensity)
J
roGFP ×10^3
Nile Red ×10^3
K
2 µm
N
L
All (n=521)
Bin (AU Intensity)
M
roGFP ×10^3
CTC
O
Dead %
****
**
***
P_S
P_L
S
S_C
S_E

Figure 7

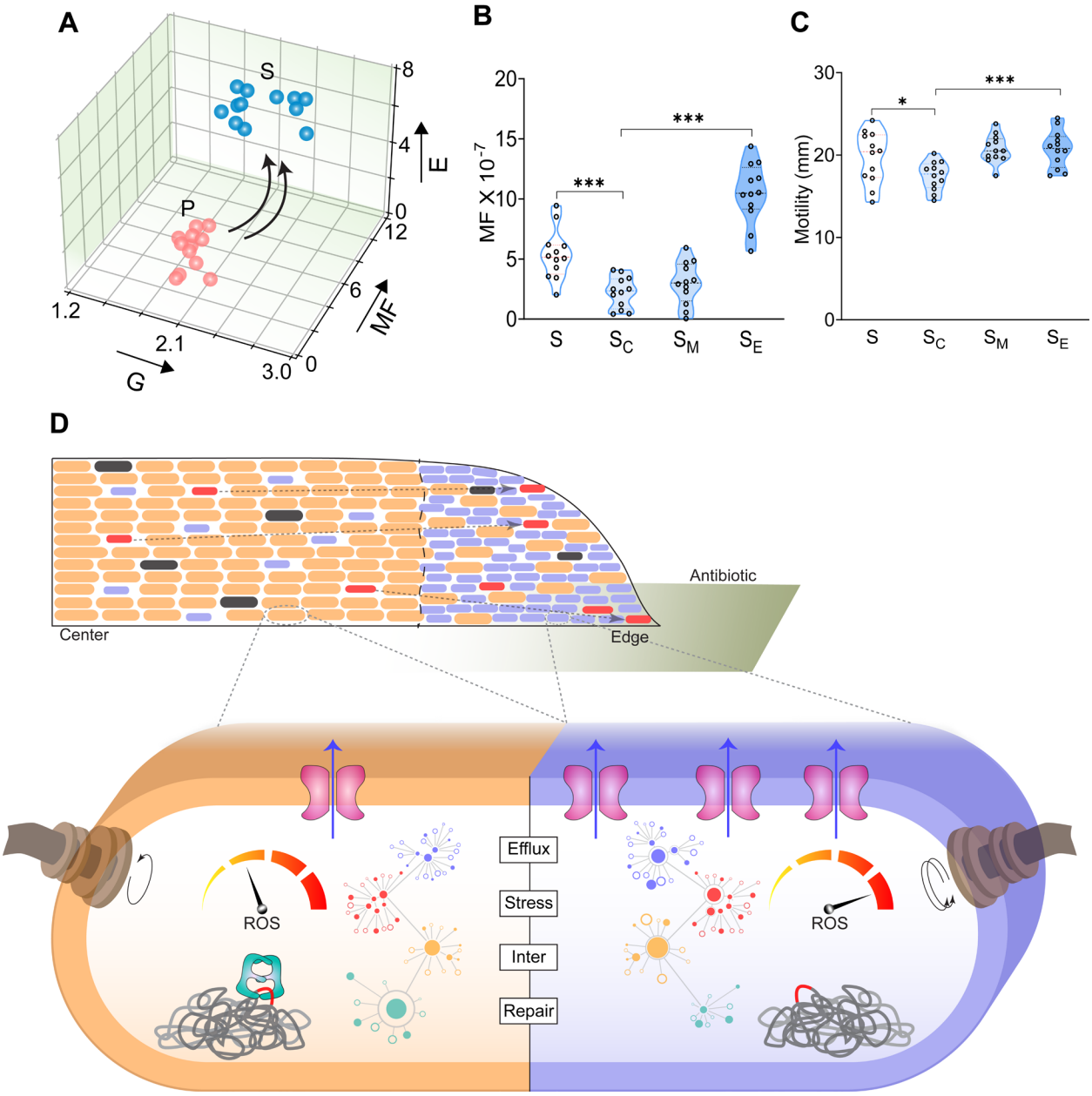
A
S
P
8
4
0
E
12
6
0
MF
1.2
2.1
3.0
G
B
MF X 10^-7
20
15
10
5
0
***
***
S
S_C
S_M
S_E
C
Motility (mm)
30
20
10
0
*
***
S
S_C
S_M
S_E
D
Antibiotic
Center
Edge
ROS
Efflux
Stress
Inter
Repair
ROS